Computational study of electrostatic focusing of aerosol nanoparticles using an einzel lens

Rayhan Ahmed, Ranganathan Gopalakrishnan

PII: S0021-8502(19)30539-7

DOI: https://doi.org/10.1016/j.jaerosci.2019.105443

Reference: AS 105443

To appear in: *Journal of Aerosol Science*

Please cite this article as: Ahmed R, Gopalakrishnan R, Computational study of electrostatic focusing of aerosol nanoparticles using an einzel lens, *Journal of Aerosol Science*, https://doi.org/10.1016/j.jaerosci.2019.105443.

Computational study of electrostatic focusing of aerosol nanoparticles using an einzel lens

Rayhan Ahmed[1] and Ranganathan Gopalakrishnan*[1]
[1]Department of Mechanical Engineering, The University of Memphis, Memphis, TN, USA

Submitted to:

Journal of Aerosol Science

*Corresponding author: rgplkrsh@memphis.edu , Tel: 1-901-678-2580, Fax: 1-901-678-4180

Abstract

This study computationally explores the possibility of focusing charged aerosol nanoparticles using electrostatics, similar to focusing of electrons and ions. A non-dimensional electrostatic focusing parameter χ_e, defined as the ratio of electrostatic potential energy to the kinetic energy of an aerosol nanoparticle, significantly determines focusing performance. The focusing device considered here is a 3-electrode electrostatic ("einzel") lens. The average focal length of the lens is seen to have an inverse power relationship with χ_e. For low values of χ_e ~ 3 in this study, the particles are seen to cross the lens axis once, while at higher χ_e multiple axis cross-over points appear. Similar to electron and ion optics, nanoparticle focusing is also limited by spherical aberration and beam divergence due to finite spread of particles in the inlet cross section of the lens and spatial non-uniformity of the focusing electric field. Other factors that influence focusing performance such as the electrostatic lens geometry, and the distribution of velocity and kinetic energy of the particles at the inlet of the lensing region are recognized, but not considered here for simplicity. In vacuum, good focusing performance (i.e.) a narrow beam of nanoparticles with minimum spherical aberration and small divergence angle is theoretically possible if χ_e<1 and if spread of particles in the inlet is confined to 20% of radius of the cylindrical lens. The effect of gas pressure is also probed to understand the degradation of focusing performance due to particle-gas interactions. It is seen that, for particles of specified size and density, a certain maximum pressure exists beyond which the device can no longer be efficiently used to focus nanoparticles. Likewise, below a certain pressure, the focusing performance is nearly independent of gas pressure, thereby enabling the selection of an operating pressure for such devices.

Keywords: nanoparticle focusing, einzel lens, charged particle optics, nanopatterning, aerosol mass spectrometry

Highlights

- Trajectory simulations are used to study the focusing of aerosol nanoparticles in a 3-electrode einzel lens.
- The focusing in vacuum is greatly influenced by a ratio of electrostatic potential energy to kinetic energy χ_e.
- The focal length is seen to vary inversely with χ_e.
- Focusing performance deteriorates with increasing gas pressure.
- A maximum pressure below which the lens needs to be operated to efficiently focus particles and a minimum pressure below which the lens behaves similar to being operated in vacuum is identified.
- Considerations for successfully selecting operating parameters (χ_e and gas pressure) are discussed.

INTRODUCTION

Focusing of aerosol (gas-phase) nanoparticles into narrow beams is motivated by applications in aerosol mass spectrometry (Deng et al. (2008); Huffman et al. (2005); Schreiner et al. (1999)), particle jet printing applications (Lin et al., 2010; Tse & Barton, 2015), micro-patterning (Di Fonzo et al., 2000; Dong et al., 2004; Qi et al., 2010),, and the fabrication of three-dimensional microstructures (Akedo et al., 1998). Murphy and Sears (1964) pioneered the generation of aerosol particle beams by flowing particles through a series of capillaries, later adopted by others (Allen & Gould, 1981; Hall & Beeman, 1976; Kievit et al., 1992; Seapan et al., 1982; Sinha & Friedlander, 1986). Although experimentally demonstrated, this method was not supported by analysis of particle motion to enable the systematic design of such focusing devices. Alternative to vacuum focusing is the use of sheath gas flow to confine particle beams to narrow cross sections by limiting their transverse diffusional broadening. While the sheath flow reduces the beam diameter effectively by a factor of ~10 (Dahneke & Cheng, 1979; Dahneke & Flachsbart, 1972), it also dilutes the particle concentration leading to decreased particle detection sensitivity for mass spectrometry or low throughput for patterning applications.

To overcome the difficulties associated with the sheath gas and to obtain higher aerosol transport efficacy than capillaries, Liu et al. (1995a) designed the aerodynamic lens that consists of a series of contractions and expansions of flow cross section achieved by the use of orifice plates. For a particle-laden flow, the aerodynamic lens provides the same focusing effect as sheath air without additional gas handling. The aerodynamic focusing of particles is based on their propensity to move towards the centerline of an axisymmetric flow when moving through successive contractions and expansions (Robinson, 1956), provided their inertia is less than the

critical inertia to avoid collision with the walls of the flow tube (Hinds, 2012). Prior to Liu et al., Fernandez De La Mora and Riesco-Chueca (2006) showed that particle inertia (described by a Stokes number that compares particle relaxation time to the fluid advection time scale) leads to focusing of particles onto a single spot and a crossover point on the axis of a flow. Their conclusions were drawn from calculated trajectories of particles in an incompressible flow through a nozzle, with Brownian motion neglected. The computational investigation described in this paper draws inspiration from Fernandez de la Mora's approach of quantifying focusing outcomes as well as the calculation of trajectories with one-way coupling to an advection field (Fernandez De La Mora, 2006; Fernandez De La Mora & Riesco-Chueca, 2006) – in that work, incompressible flow field was employed, while we investigate the effect of electrostatic field in vacuum and at finite pressures (without a systematic fluid flow field). The minimum beam width achieved using the inertial focusing method of Liu et al. (1995a) approaches ~0.4 mm, that increases with decreasing particle size as demonstrated using spherical dioctyl sebacate particles in the range of ~50 – 250 nm (Liu et al., 1995b). Several designs of aerodynamic lenses have been used to effectively collimate nanoparticles in the range of 100–900 nm (Schreiner et al., 1999), 340–4000 nm (Schreiner et al., 1998), 60–600 nm (Zhang et al., 2004), 3–30 nm (Wang et al., 2005), 30–300 nm (Lee et al., 2008), 5–50 nm (Lee et al., 2009) and 30 nm–10 μm (Lee et al., 2013). The beam width produced by this method is limited by Brownian motion and lift forces on the particles during expansion through the orifices and the exit nozzle of the lens. Overcoming the Brownian limit of beam broadening is theoretically impossible without the application of radial forces by external means (such as electric fields for example). Thus, reduction of beam width beyond those achieved by the aerodynamic lens has been challenging and has not been accomplished so far.

Alternate to the inertial particle focusing mechanism of the aerodynamic lens, several attempts have been made to use electrostatic and electrodynamic forces or a combination of both fluid and electric forces to focus particles. Electron and ion focusing devices using applied electric fields have been harnessed for many applications such as electron microscopes, cathode ray tubes, ion beam milling apparatus and drift tube mobility spectrometry (Cumeras et al., 2015; Fernández-Maestre, 2012; Oberreit & Hogan Jr, 2015). The ion/electron trajectories in these devices are manipulated using a series of ring/planar electrodes with an applied voltage gradient to confine them to a narrow region around the axis. The analogous use of electric fields to focus aerosol nanoparticles could potentially mitigate beam broadening by Brownian motion and be instrumental in producing narrow beams than is currently possible using inertial focusing alone. The charge and electrical mobility (which is dependent on the gas pressure) of particles determine their response to an applied electric field. Electric fields have been used numerously to manipulate the trajectories of aerosol particles for measurement and patterning. Knutson and Whitby (1975) developed the differential mobility analyzer that spatially separates particles based on their electrical mobility or size (for spheres). The experimental verification Liu et al. (1995b)'s design of aerodynamic lens (Liu et al., 1995a) used electrostatic fields to deflect charged particles to measure their nominal velocity in a focused beam. Kane et al. (2001) used an electrostatic lens to concentrate nanoparticles before introducing into the time-of-flight detector of a mass spectrometer for improved sensitivity. They have observed that electrostatic focusing increases the hit rate (sensitivity) by increasing the overlap of the laser beam with the particle beam. The deposition of charged nanoparticles (<5 nm) of diverse materials using photoresists (for selective area deposition) and external biasing of voltages has enable the creation of nano-

patterns and are successful demonstrations of the utility of electric fields to control particle motion advantageously (Choi et al., 2015; Kim et al., 2006; Krinke et al., 2002; Lin et al., 2010; Park et al., 2013; You & Choi, 2007; You et al., 2010).

Masuda et al. (1972) used a set of parallel cylindrical electrodes, separated by insulating spacers and connected to an alternating voltage source that produced a spatially periodic electric field in the focusing region. Charged aerosol particles were shown to have periodic motion along the curved lines of force and were repulsed from the electrode due to the action of centrifugal force and electric force. Based on the different electrode configurations, the particles can either levitate or levitate and accelerate simultaneously along the lens axis. Based on the same methodology, Holm and Addison (1991) designed a cone frustum shaped screen having an entrance and exit diameter of 7.0 cm and 2.5 cm respectively with a length of 17.0 cm for electrodynamic focusing of charged particles and achieved minimum beam width ~ 1 mm. They have observed that 5.2 μm particles could be focused to ~2 – 4 mm beam widths for electric elementary charges of 2000 to 6000, positive or negative charges on the particles. As aerosol particles are much heavier and have lower velocities than electrons and ions, it is conceivable that they require considerably higher number of electric charges to respond to the applied field ($\vec{F} = q\vec{E}$).

Heise and Rang (1949) have used a simple 3-electrode einzel lens to focus electron beams experimentally, analogous to light. An einzel lens is made of three ring electrodes (separated by insulating spacers), with the first and third electrodes held at the same voltage (and of the same length) while the second electrode is held at a different voltage to create a voltage gradient for focusing. The numerical calculations of electron focusing using einzel lenses that

relate the focal length and the operating parameters (voltage and geometry) developed by Adams and Read (1972) have been used numerously to design charged particle focusing devices (Chang et al., 1996; Odenthal, 1991). Computational studies have been used to understand electrostatic particle deposition and inspires our use of trajectory simulations to parameterize focusing using electrostatic fields (Rusinque et al., 2019). A systematic exploration of the motion of charged nanoparticles particles to understand electrostatic focusing using a cylindrical einzel lens with a simple 3-electrode geometry is carried out in this study. Motivated by ion and electron focusing using einzel lenses, it is desirable to deduce the operating parameters (particle velocity and charge, strength of electric fields and gas pressure) for successful focusing of nano- and micro-particles beyond the Brownian diffusion limit. This study, using trajectory simulations, computationally explores the electrostatic focusing of aerosol nanoparticles to understand the effect of particle parameters (material, kinetic energy/velocity, size, number of charges), lens geometry, operating voltage/applied electric field and gas pressure on focusing performance (quantified by the focal length, spherical aberration and divergence angle of particle beams). The comparison between the electric potential energy of the particle to kinetic energy determines the ease with which they are deflected towards the lens axis by the applied electric field. The thermal energy of the particles as well as the drag exerted by the gas medium on their motion are also important in determining focusing outcomes. We also identify conditions in which the spherical aberration and divergence angle of the focused beam can be minimized and deduce the upper limit of gas pressure at which an einzel lens acts as a focusing device without significant distortion by collisions between particles and background gas molecules. Lastly, we elucidate qualitative relationships between focal length, spherical aberration and the divergence angle with

the ratio of the electric potential energy to the kinetic energy of the particles, the particle Knudsen number as well as particle diameter and material density.

COMPUTATIONAL METHODS

Electrostatic potential in the einzel lens: The electrostatic focusing of nanoparticles using a 3-electrode einzel lens is investigated through particle trajectory simulations. Assuming that the concentration of charged aerosol particles injected into the focusing region is low, the distortion of the electric field by space charge due to the particles is neglected and a one-way coupling is assumed to exist between the electric field due to the einzel lens and particles. The electrostatic potential φ (and the electrostatic field $\vec{E} = -\nabla\varphi$) inside the einzel lens is obtained by solving the Poisson equation, assuming the space charge is zero, using the commercial software COMSOL®:

$$\nabla^2\varphi = 0 \ldots (1)$$

Eq. 1 is solved in an axisymmetric einzel lens geometry, shown in **Figure 1-A**, representing a cylindrical einzel lens whose dimensions are expressed in multiples of the radius of the lens R. The lens geometry consists of three cylindrical electrodes of identical radius. The length of the first electrode (L_1) and third (L_3) electrode was chosen to be $4.5R$ by trial and error such that the particles enter and leave the lens under electric field-free conditions $\vec{E} \approx 0$. The length of the second electrode (L_2) is set to $1.5R$ for simplicity. The length of the dielectric spacer between the electrodes δ defines the strength of the electrostatic field existing in the focusing region (Adams & Read, 1972; Ciric et al., 1976). Although there are multiple choices for δ, we again set $\delta = R$ for simplicity. All results presented in the reminder of this article correspond to these set of geometrical choices to probe the effect of applied voltage, gas pressure and particle parameters (size, density, and incoming velocity). The effect of lens geometry, though important, is not the focus of this computational investigation of electrostatic focusing. The electrostatic

potential φ and electric field $\vec{E}$ components were exported from COMSOL® to particle trajectory simulation routines to investigate focusing in vacuum and at finite gas pressures.

Particle trajectory simulations in vacuum ($P = 0$)*:* The trajectories of nanoparticles inside the einzel (assumed to be operated in vacuum) are calculated by solving Newton's second law of motion:

$$\frac{d\vec{v}}{dt} = \chi_e \vec{E} \ldots (2)$$

Eq. 2 was integrated in time using the velocity-Verlet numerical scheme (Verlet, 1967):

$$\vec{x}(t + \Delta t) = \vec{x}(t) + \vec{v}(t)\,\Delta t + \frac{1}{2}\,\chi_e \vec{E}\big(\vec{x}(t)\big)\left(\frac{R}{\delta}\right)\Delta t^2 \ldots (3a)$$

$$\vec{v}(t + \Delta t) = \vec{v}(t) + \frac{1}{2}\,\chi_e \left(\vec{E}\big(\vec{x}(t)\big) + \vec{E}\big(\vec{x}(t + \Delta t)\big)\right)\left(\frac{R}{\delta}\right)\Delta t \ldots (3b)$$

Here, $\vec{x}(t)$ and $\vec{v}(t)$ are the non-dimensional position and velocity vector of a particle, respectively. All lengths are expressed in multiples of the electrode radius R, while velocities are scaled using U_o, the initial velocity of the particles at the entrance of the einzel lens. $\vec{E}(\vec{x})$ is the non-dimensional electrostatic field obtained by normalizing the electric field exported from COMSOL® (with unit of V/m) by the nominal electric field calculated as $\frac{\Delta V}{\delta}$. Here ΔV is the applied voltage difference across the tube electrodes, $\Delta V = V_1 - V_2 = V_3 - V_2$. $\chi_e \equiv \frac{n_p e \Delta V}{m_p U_o^2}$ is a ratio of the electrostatic potential energy to the initial kinetic energy of the particle carrying n_p units of electronic charge e, of density ρ_p and having a mass of m_p. The particles are assumed to be spherical with a diameter of d_p such that $m_p = \frac{\pi}{6}\rho_p d_p^3$. χ_e compares the electrostatic potential energy of the particles to the kinetic energy (inertia). **Table 1** shows the variation of χ_e as a function of d_p and n_p for different materials. The values of χ_e were calculated considering a particle velocity of $U_o = 100$ m/s and a voltage difference $\Delta V = 1000\ V$ across the electrodes of

the einzel lens. Our choice of 100 m/s is based on the measured exit velocities of particles from focusing devices such as the aerodynamic lens (Liu et al., 1995b), that will be presumably used for accelerating and focusing particles that can be further improved using an einzel lens in series. For a 100 nm gold particle, $\chi_e = 0.0016 - 0.1584$ as n_p is varied from 1 – 100. The maximum value of χ_e for a given material and particle size is limited by the charge limit n_L set by the self-generated field strength for spontaneous emission of electrons or positive ions from the particle surface assuming an ion evaporation mechanism (Gamero-Castaño & Mora, 2000; Thomson & Iribarne, 1979):

$$n_L = \frac{d_p^2 E_L}{4K_E e} \ldots (4)$$

E_L is the material-dependent surface field strength required for spontaneous emission of electrons or positively charged ions. Further, the emission field strength is also dependent on the composition of the charge carrier. For electrons, typical values of $E_L \sim 10^8\ V/m$, and for positive charged ions $E_L \sim 10^{10}$ V/m. The electrostatic constant of proportionality $K_E = 9.0 \times 10^9$ Nm^2C^{-2}. The maximum value of χ_e for a 100 nm gold particle is 2.4755 based on the charge limit for gold. Similarly, for the highest value of χ_e for a 10 nm silicon particle is 210.12 based on the corresponding charge limit. Therefore, it is clear that χ_e increases with the inverse of mass to charge ratio of the aerosol nanoparticle. For an electron with a velocity of ~10^7 m/s and voltage difference of 1000 V across electrodes, $\chi_e \sim 1.76 - 0.0176$ signifies the possibility of focusing particles like electrons and ions by einzel lenses. In results that will be presented in subsequent sections, we probe the effect of χ_e on the focusing performance of the einzel lens in vacuum and at finite gas pressure.

Particle trajectory simulations at finite pressure ($P \neq 0$)*:* In addition to electrostatic interactions quantified by χ_e, the finite gas pressure in focusing devices leads to hydrodynamic drag on particles exerted by the gas medium and Brownian motion due to collisions with gas molecules. At low pressures considered here, Brownian motion is neglected. This assumption is justified posteriori by the lack of significant difference between trajectories simulated with and without Brownian motion. Particle trajectory simulations were carried out by solving the non-dimensional equation of motion considering only the hydrodynamic drag and electrostatic force on the particles:

$$\frac{d\vec{v}}{dt} = \chi_e \vec{E} - \frac{3}{4}\frac{C_H\, \rho_g\, \delta\, |\vec{v}|^2}{\rho_p d_p}\frac{\vec{v}}{|\vec{v}|} \quad \ldots (5)$$

C_H is the drag coefficient and for subsonic particle velocities, the Henderson correlation (1976) was used:

$$C_H = 24\left[1.77\,\frac{S}{Kn_p} + S\left\{4.33 + \left(\frac{3.65 - 1.53\frac{T_p}{T_g}}{1 + 0.353\frac{T_p}{T_g}}\right) \times \exp\left(-\frac{0.438}{Kn_p}\right)\right\}\right]^{-1}$$
$$+ \exp\left(-0.447\sqrt{\frac{Ma_p Kn_p}{\gamma^{0.5}}}\right)\left[\frac{4.5Kn_p + 0.38\left(0.053\,S + 0.639\,\sqrt{Kn_p S}\right)}{Kn_p + 0.053\,S + 0.639\sqrt{Kn_p S}}\right.$$
$$\left. + 0.1Ma_p^2 + 0.2Ma_p^8\right] + 0.6S\left[1 - \exp\left(-0.798\frac{Kn_p}{\gamma^{0.5}}\right)\right] \quad \ldots (6)$$

where $Kn_p \equiv \frac{2\lambda_g}{d_p} = \frac{Ma_p}{Re_p}\sqrt{\frac{\gamma\pi}{2}}$ is the Knudsen number of particle, Re_p is the Reynolds number based on particle diameter, $Ma_p = \frac{v_p}{c}$ is the Mach number of the particle defined as particle speed v_p to the speed of sound c, λ_g is the mean free path of the gas molecules, molecular speed ratio $S = Ma_p\sqrt{\gamma/2}$ (γ is the ratio of gas specific heats at constant pressure and constant

volume). For the pressures considered here, most of the calculations fall in the free-molecular limit of $Kn_p \to \infty$. Finally, T_p is the particle temperature assumed to be equal to the gas temperature T_g (i.e.) $\frac{T_p}{T_g} = 1$. Eq. 5 was solved considering Henderson's correlation (eq. 6) using a leap-frog variant of the velocity-Verlet method with damping terms to capture the effect of drag:

$$\vec{x}(t + \Delta t) = \vec{x}(t) + \vec{v}(t)\Delta t + \frac{1}{2}\Delta t^2 \vec{a}\big(\vec{x}(t), \vec{v}(t)\big) \ldots (7a)$$

$$\vec{v}^I = \vec{v}(t) + \vec{a}\big(\vec{x}(t), \vec{v}(t)\big)\Delta t;\ \vec{a}^I = \vec{a}(\vec{x}(t + \Delta t), \vec{v}^I) \ldots (7b)$$

$$\vec{v}^{II} = \vec{v}(t) + \frac{\big[\vec{a}\big(\vec{x}(t), \vec{v}(t)\big) + \vec{a}^I\big]}{2}\Delta t;\ \vec{a}^{II} = \vec{a}(\vec{x}(t + \Delta t), \vec{v}^{II}) \ldots (7c)$$

$$\vec{v}(t + \Delta t) = \vec{v}(t) + \frac{\big[\vec{a}\big(\vec{x}(t), \vec{v}(t)\big) + \vec{a}^{II}\big]}{2}\Delta t \ldots (7d)$$

where $\vec{a}\big(\vec{x}(t), \vec{v}(t)\big) = \chi_e \vec{E}\big(\vec{x}(t)\big) - \frac{3}{4}\frac{C_H \rho_g \delta |\vec{v}|^2}{\rho_p d_p}\frac{\vec{v}}{|\vec{v}|}$ to include acceleration due to both electrostatic force and hydrodynamic drag force.

Particle trajectory simulations are analyzed in subsequent sections to elucidate electrostatic particle focusing using einzel lenses. For cases considering focusing in vacuum ($P = 0$), equations 3a and 3b were used to obtain particle position and velocity as a function of time. Likewise, equations 7a – 7d were used for finite pressure cases considering drag due to gas molecules and electrostatic force on the particles. **Figure 1-B** illustrates the parameters that influence, and metrics to quantify focusing performance. In the trajectory simulations described in this paper, charged particles are introduced into the simulation domain with a dimensionless velocity of 1.0, parallel to the optic axis. Particle focusing through the einzel lens is like electron/ion optics wherein charged particles respond to the applied electrostatic field and are deflected towards the center line. The "reference plane" shown in **Figure 1-B** is used as the

reference datum to measure all lengths subsequently discussed and the center line of the cylindrical electrodes is termed as optic axis. The point of first cross-over on the optic axis is referred to as focal point (analogous to electron/light optics) and the distance of focal point is termed the focal length f_L – the particle trajectories are assumed to be axi-symmetric. The initial radial distance of the particles from the optic axis, B_o at the entrance of the einzel lens is varied from 0 to 1 (measured in multiples of R, the radius of the cylindrical electrode). Throughout this study, the particles at the entrance of the lens are assumed to have a velocity *parallel* to the optic axis - the angle α_i (not shown on **Figure 1-B**) between the initial velocity and the optic axis is set to zero. We elect to focus on quantifying the principal focusing parameters χ_e and B_o and defer the variation of the incoming particle velocity direction α_i to future investigations. As depicted in **Figure 1-C**, the trajectory of a particle starting close to the optic axis is referred to as the paraxial trajectory ($B_o = 0.005$ in this work). Likewise, the trajectory of a particle starting close to the electrode is referred to as the peripheral trajectory ($B_o = 1$). The angle between a particle trajectory and the optic axis after cross-over is referred to as the divergence angle α_o. The point of cross-over of the paraxial trajectory with the optic axis is the paraxial focal point. The transverse spherical aberration Δr is the radial distance of a particle measured in the plane of the paraxial focal point. The effect of χ_e and B_o on focusing performance quantified by focal length f_L, divergence angle α_o and the transverse spherical aberration Δr is investigated computationally in the reminder of this paper. The charged particles are assumed to be dilute in concentration inside the einzel lens – hence, all particle-particle interactions are neglected in considering their trajectories through the lensing region and at the point of cross-over. We note that the electrostatic repulsion between like-charged particles will restrict their focusing onto a

single point and will cause a finite focal volume through which all the particles nominally pass through. In this investigation, we also elect to ignore this effect for simplicity.

RESULTS AND DISCUSSION

Effect of χ_e and B_o on particle focusing in vacuum: 100 particle trajectories were calculated for each χ_e and for various values of the radial distance of the particle from the optic axis at the entrance of the einzel lens, B_o varied between 0.0 to 1.0. Only trajectories for $B_o \leq 0.5$ are included in **Figures 2** and **4** for the sake of clarity and to illustrate specifically, the cross-over of particles starting at different radial locations on the starting plane. As χ_e increases from zero, the particles are deflected increasingly strongly towards the optic axis. **Figure 2-A – 2-D** shows the dependence of the focal length f_L on χ_e in the range of 0.01 – 1. The first cross-over point shifts closer to the reference plane as χ_e increases. This behavior is similar to electron trajectories in an einzel lens for different focusing electric field strengths as observed by Heise and Rang (1949) and shown in **Figures 3-A** and **3-B**. **Figure 3** is a reproduction from the original work of Heise and Rang that highlights the similarity between experimentally-observed electron trajectories and aerosol particle trajectories calculated here. Heise and Rang further observed that for higher strengths of the focusing electric field, the electron trajectories cross the optic axis multiple times as shown in **Figures 3-C** and **3-D**. From **Figure 4**, representing calculated particle trajectories for $\chi_e = 3 - 275$, it can be observed that for $\chi_e = 3$ the particle trajectories cross the optic axis once near the center of the lensing region and for a second time further downstream. For $\chi_e = 4$ and 10, the first cross-over points are closer to the reference plane and the second cross-over points have also shifted towards the lensing region compared to $\chi_e = 3$. For $\chi_e = 275$, three cross-over points are found in the particle trajectories. A wide dynamic range of χ_e could be obtained by manipulating either the number of charges on the particle n_p, operating voltage difference ΔV and the design of the einzel lens (principally, the electrode spacing distance δ) as shown in **Table 1**.

Figures 2 and 4 show that charged nanoparticles can be focused analogous to electrons/ions across a wide range of particle size and material, thus making the einzel lens a promising mechanism for particle focusing. The number and location of multiple axis cross-overs shown here are dependent also on the dimensions of the simulation domain and geometric design of the einzel lens. Nevertheless, the trajectory simulations carried out here offer proof of concept for focusing aerosol nanoparticles onto a single spot using einzel lenses for applications such as surface nanopatterning and mass-spectrometry.

The focal length of the particle beam depends on χ_e, B_o and the angle between the velocity vector and the optic axis α_i at the inlet of the einzel lens. In this study, for simplicity, we have set $\alpha_i = 0$ to focus on the effect of χ_e, B_o (i. e.) $f_L = f_L(\chi_e, B_o, \alpha_i = 0)$. For a given χ_e, the average focal length $\langle f_L \rangle$ is calculated based on 100 particle trajectories with B_o distributed randomly between 0 and 0.1. As seen in **Figure 5-A**, the average focal length $\langle f_L \rangle$, shown as a solid line, decreases with increasing χ_e which offers an operating map to select χ_e to achieve a targeted focal length or particle cross-over distance. The inverse relationship between $\langle f_L \rangle$ and χ_e is approximately represented as:

$$\langle f_L \rangle \approx A\chi_e^{-C} \quad \ldots (8)$$

where fit constant A=5.687 and C=1.103 are specific to the dimensions of the domain used here but reveal a general inverse power-law relationship between focal length and focusing voltage expressed in terms of χ_e. Also shown on **Figure 5-A**, are the maximum and minimum focal lengths corresponding to the paraxial ($B_o = 0.005$) and peripheral ($B_o = 1$) particle trajectories. It is seen that the difference between the extreme values of the focal lengths is up to ~20%

compared to the average focal length at low χ_e and the difference decreases with increasing χ_e. The minimum and maximum focal lengths shown on **Figure 5-A** reveal that at $\chi_e = 0.34$, the difference is ~20% and at $\chi_e = 3$, the difference is ~5%. This is also confirmed by **Figure 5-B**, that shows the variation of the focal length f_L as a function of the initial radial distance of the particle B_o for various χ_e values. We note that, for $B_o < 0.2$, the difference between the two focal lengths is small compared to the average focal length $\langle f_L \rangle$ – in practical terms, particles that start within 20% of the radius of the cylinder could be focused effectively onto a tight spot with minimum beam spreading.

Constraints in particle focusing using single Einzel lens: The spatial non-uniformity in the focusing electric field of the einzel lens and finite spread of the particle radial location at the inlet plane of the lens causes different degrees of deflection of the particle trajectories. This leads to the particles crossing the optic axis at different points that are located on planes that are parallel (axial direction) and perpendicular (radial direction) to the optic axis. The spread of the focal points *along* the optic axis, known as the longitudinal spherical aberration Δf_L (depicted in **Figure 1-C**), was quantified in **Figure 5-A** using the average focal length with maximum and minimum bounds. The spread of the focal point in the radial direction (*perpendicular* to the optic axis) is defined as the transverse spherical aberration Δr (depicted in **Figure 1-C**). We calculate Δr as the radial distance of a particle trajectory measured in the plane of the paraxial focal point. Along with the focal length, the transverse spherical aberration Δr is also used to quantify focusing performance as a function of χ_e, B_o with $\alpha_i = 0$ i.e. $\Delta r = \Delta r(\chi_e, B_o, \alpha_i = 0)$. Like light and electron optics, particle focusing is also limited by spherical aberration (Abdelsalam & Stanislas, 2017; Weißbäcker & Rose, 2001). The spread of the particle beam after cross-over is

quantified by the divergence α_o that is the angle between the optic axis and the particle trajectory measured in the plane of the paraxial focal point (like the transverse spherical aberration definition). Likewise, $\alpha_o = \alpha_o\ (\chi_e, B_o, \alpha_i = 0)$ is analyzed from trajectory simulations.

Figure 6-A shows the variation of the transverse spherical aberration for various initial radial locations of the particle B_o. It is seen that particles that start near the wall (where the electric field is the strongest) are deflected the most and have high Δr. Also, for particles that start within approximately 20% of the radius of the lens (i.e.) $B_o < 0.2$, the transverse spherical aberration is practically negligible. This allows the recognition of an important operating insight which will allow the minimization of beam width and broadening during focusing. Also, as χ_e increases, Δr decreases for identical B_o values, indicating tighter focusing by the electric field. The maximum transverse spherical aberration Δr_{max} (the radial location of the outermost particle trajectory from the optic axis) decreases with increase in χ_e as shown in **Figure 6-B**. As in the case of eq. 8 for the average focal length, the regression relating Δr_{max} (corresponding to $B_o = 1$) and χ_e are also system-specific but indicate a non-linear dependence of the Δr_{max} on the (non-dimensional) focusing voltage χ_e. **Figure 6-C** shows the variation of α_o with B_o and χ_e. It is clearly seen that α_o, and subsequently the beam broadening after cross-over, can be minimized by confining the particles entering a lens to near the optic axis (for example, $B_o < 0.2$). α_o also increases with χ_e, indicating a trend opposite to that of Δr. The maximum divergence angle $\alpha_{o,max}$, plotted in **Figure 6-D**, increases with χ_e. Thus, to obtain a tight focal point the selection of an optimal set of B_o and χ_e is required to minimize *both* Δr and α_o. Depending on the desired location of the focal point (which may be dictated by the position of the substrate or a detector of aerosol particles such as a Faraday cup electrometer), the selection of B_o and χ_e requires

optimization considering the trends shown in **Figures 6-A** and **6-C**. Additional trajectory simulations with the specific dimensions of the focusing device along with the location of the substrate will be necessary to determine the optimal χ_e.

In addition to B_o, χ_e and α_i (whose effect we have deferred to future investigations and set $\alpha_i = 0$ currently), the lens geometry (Daimon et al., 2010) also plays an important role in determining $f_L, \Delta r, \alpha_o$. The length of the electrodes and the width of the dielectric spacing determine the nominal field strength ~ $\frac{\Delta V}{\delta}$ and the gradient in the electric fields (that determine the location of cross-over) in the simulation domain. The effect of lens dimensions on focusing also needs to be investigated in the future. From our trajectory calculations, it is evident that for $\chi_e < 1$, the focal point is sufficiently far from the lensing region (where the electric field is non-zero). For a practical device, it is necessary that any material surface be sufficiently far away from the focusing electrodes to prevent distortion of the field lines and particle trajectories. From the parametric study of B_o, χ_e on focusing, we establish proof of concept for focusing charged aerosol nanoparticles using an einzel lens in vacuum. However, practical devices are operated at finite low pressure that requires an understanding of the interaction between the particles and the background gas in addition to electrostatic interactions. In the next sub-section, we focus on the effect of gas pressure on particle focusing.

Effect of finite pressure on particle focusing: Maintaining a high level of vacuum is a prerequisite for successfully operating charged particle focusing systems (Matsui et al., 1995) as particle-gas molecule collisions degrades or destroys focusing performance due to systematic hydrodynamic drag and stochastic Brownian motion. The effect of pressure is parameterized by

the particle Knudsen number Kn_p that is inversely proportional to gas pressure as was previously defined in the *Methods* section. At low pressures, the effect of Brownian motion is expected to be minimal and vanish in the limit of gas pressure $\rightarrow 0$. To assess the importance of Brownian motion at low pressures (~0.001 – 400 Pa), we elected to compare trajectories that were computed using two approximations: 1) that includes drag as described by Henderson's model (equations 5 and 6, with solution given by equations 7a – 7d) but neglects Brownian motion and 2) the Langevin equation of motion (Chandrasekhar, 1943; Langevin, 1903) that includes drag and Brownian motion. The Langevin equation is strictly valid only in the continuum regime of particle transport (i.e.) at high pressures wherein the particles relax instantly to their thermal velocities due to high number of collisions with gas molecules (Mazur & Oppenheim, 1970). The Langevin equation was used to capture the effect of Brownian motion on particle trajectories through the einzel lens (details of the numerical method used is described in detail in the Supplemental Information, SI). Trajectory calculations were obtained for identical gas pressure and focusing parameter χ_e for the two cases – with and without Brownian motion. We note that the Langevin formulation assumes that the drag is linearly proportional to the velocity of the particle relative to the gas medium in the limit of $Re_p, Ma_p \rightarrow 0$, while Henderson's model (derived for high Re_p, Ma_p flows around spherical objects) assumes that drag is proportional to the second power of velocity. Trajectories were calculated for 10 nm, 50 nm, and 100 nm gold particles for pressures 0.001 – 400 Pa all corresponding to $\chi_e = 0.3$ and are presented in Figures 7, 8, and 9, respectively. In each of these figures, two sets of computed trajectories are shown – the top panels correspond to calculations with the Henderson correlation and the bottom panels using the Langevin equation with the value of the gas pressure noted above each panel. In addition to the non-dimensional ratios χ_e and Kn_p, the trajectories are also examined to delineate

the dependence of focusing outcomes on size-dependent particle diffusion. Figure 7 (showing trajectories of 10 nm gold particles as a function of pressure and at $\chi_e = 0.3$), demonstrates a marked difference between Henderson and Langevin-derived trajectories. Henderson correlation, that neglects particle diffusion and Brownian motion, shows that at 100 Pa, the einzel focusing of charged aerosol particles ceases to be useful and does not lead to particle cross over on the axis. When diffusion is included, via the Langevin equation, particle focusing is only marginally successful at 0.1 Pa and is significantly poor at greater pressures. We also note that, at 0.001 Pa, Langevin equation also predicts particle trajectories that terminate at the wall. Contrastingly, the Henderson correlation-determined trajectories at the same pressure are very similar to vacuum (see **Figure 2-C**). This is attributed to the breaking down of the Langevin model – the approximation of a fluctuating force function to mimic particle-gas molecule impacts that are inherently discrete in nature (Mazur & Oppenheim, 1970) at very low pressures. Hence, we conclude from this comparison that while the effect of Brownian motion and particle diffusion may be neglected *below* a certain pressure, which would be the operating pressure of an einzel lens based focusing system, such an operating pressure is dependent on particle size and needs to be established through trajectory calculations with an appropriate computational model (Henderson/Langevin or other) and specific lens geometry. This assertion is further supported by the trajectories of 50 nm gold particles at various pressures as shown in Figure 8 (again, top panels computed using Henderson's correlation and bottom panels using Langevin equation). In this case, we see that up to 200 Pa, particle trajectories are minimally influenced by Brownian motion and diffusion – as evidenced by similar qualitative features between trajectories calculated using both the models. For 100 nm gold particles, the operating pressure of the einzel lens may be as high as 400 Pa (**Figure 9**). These trajectories (**Figures 7 – 9**), show the increase

of focal length as pressure decreases and the asymptotic behavior of the same as pressure →0. They also show us that the maximum operating pressure of the einzel lens system must be selected taking into account particle Brownian motion– that considerably influences 10 nm sized particle focusing than 100 nm or larger sized particles comparitively. The trajectories of particles at pressures of 0 Pa (vacuum), 0.001 Pa and 0.1 Pa are nearly identical as well for 100 nm particles. As pressure is increased, focal length reduces and eventually as pressure exceeds 10 Pa for 10 nm particles, 200 Pa for 50 nm particles and 400 Pa for 100 nm particles, the focusing effect diminishes and gas molecule-particle drag prevents particles from crossing the optic axis at a single focal point. The qualitative features seen in these trajectory calculations are quantified by the average focal length $\langle f_L \rangle$. The initial radial location of the particles B_o was varied uniformly from 0 to 1 and the average focal length $\langle f_L \rangle$ calculated from both Langevin equation and eq. 5 (with Henderson's drag correlation, eq. 6) is plotted in **Figure 10**. At pressures 10 – 400 Pa, or particle Knudsen number $Kn_p < 1.5 \times 10^4$, the focal length according to both the models differ by no more than 13 % indicating that the contribution of Brownian motion is not significantly high at such low pressures. Above a certain pressure (or below a certain Kn_p), the particles do not cross the optic axis but are lost to the walls due to Brownian motion and electrostatic force. This regime of pressure is clearly unsuitable for operating the electrodes as a focusing device. Hence, a certain maximum pressure is hypothesized to exist for particles of a given size and material. Below this maximum pressure, focusing is reasonably accurately described by the Henderson's equation (that considers only drag force) without undue computational complexity. Also, from **Figure 10**, it is evident that below pressure 1 Pa (or $Kn_p > 1.5 \times 10^4$), the predictions of both Langevin and Henderson's equation are nearly the same, further vindicating the neglect of Brownian motion at low pressures or high vacuum

conditions. Based on this sensitivity analysis, subsequent results discussed in this paper are derived using Henderson's equation only for simplicity and may be considered to be accurate for particles 50 nm and larger. For smaller particles, a detailed analysis including Brownian motion is necessary and may be taken up in the future.

To probe the effect of both χ_e and gas pressure, trajectory calculations for $\chi_e = 0.3 - 1.0$ were carried out in the pressure range of 0.001 – 400 Pa, that corresponds to $Kn_p = 1.38 \times 10^8 - 3.40 \times 10^2$. To realizes these parameters, 100 nm gold particles were introduced into the einzel lens. The incoming velocity was set to 100 m/s and number of charges on each particle was adjusted to obtain a targeted χ_e. Also, B_o was varied between 0 to 0.2 to minimize spherical aberration. The average focal length $\langle f_L \rangle$ as a function of χ_e and Kn_p plotted in **Figure 11-A** shows three operating regimes based on gas pressure. At pressures > 400 Pa, there is no focusing effect, acting as the upper limit on gas pressure to operate the specific design of einzel lenses considered here. At intermediate pressures, wherein gas drag on the particles is not negligible, the focal length steeply rises with decreasing pressure and converges to an asymptotic value (that is identical to the focal length calculated in vacuum). Below a certain pressure, the focal length is independent of gas pressure, further showing the negligible effect of the gas medium on focusing and establishing an operating pressure for einzel lens focusing of particles. The curves shown in **Figure 11-A**, also depend on more parameters than just χ_e and Kn_p. From **Figure 11-B**, wherein the particle size and density (material) are systematically varied, it is clear that these trends are universal for nanoparticles. The maximum operating pressure (below which focusing is possible) is size and material dependent as shown in **Figure 11-B**. However, the pressure below which the particles behave like in vacuum, is dependent on size as evident from the trends seen from Figure

7 – 9. In practical terms, the selection of a low pressure and a targeted gas flow rate into the einzel lens allows the selection of a suitable pumping system and operation of the lens for focusing a wide range of sizes and materials. Lastly, in addition to average focal length $\langle f_L \rangle$, the maximum spherical aberration Δr_{max} and maximum divergence angle $\alpha_{o,max}$ are also influenced by gas pressure as shown in **Figure 12-A** and **12-B**, respectively. Similar to the change in average focal length with pressure, the maximum spherical aberration Δr_{max} (**Figure 12-A**) also decreases with increase in pressure for a certain range, here 10 – 400 Pa. Below, 10 Pa, Δr_{max} can be seen to be independent of gas pressure and material. This allows the realization of tight spot sizes if such an einzel lens were to be used for nanopatterning. However, in **Figure 12-B**, the maximum divergence angle $\alpha_{o,max}$ shows a contrasting trend to Δr_{max} in the 10 – 400 Pa pressure range, $\alpha_{o,max}$ increases with increasing pressure. At low pressure, below 10 Pa, $\alpha_{o,max}$ is also insensitive to the gas pressure. For example, at $\chi_e = 0.3$, the difference between $\alpha_{o,max}$ in vacuum and at ~100 Pa is nearly 25%. For a pressure of 400 Pa, the difference is ~150%. This increase non-linearly decreases with χ_e but remains significant throughout the χ_e range considered. At $\chi_e = 1.0$, the increase in $\alpha_{o,max}$ is ~20%. Therefore, to obtain tight spot sizes for patterning or for increasing the sensitivity of time-of-flight detectors, the placement position of the target surface is crucial. It is most advantageous if the surface is placed at the focal point of the particles (assuming focal point is in the electric field free region and the placed surface does not distort the electric field of the lens). However, if the surface is placed downstream of the focal point (for practical reasons), a large divergence angle will cause significant broadening of the beam after crossover. The diameter of the spot scales with the distance between the focal point and the target surface times the tangent of the maximum divergence angle. Thus, it can be seen that a high operating pressure significantly effects the focusing performance (focal length,

beam broadening and divergence angle) and it can even destroy the focusing effect of the lens by reducing the particle inertial velocity by dissipation of kinetic energy. This can lead to significant beam broadening or spot enlargement, reducing the gains of using an einzel lens for focusing particles.

CONCLUSIONS

From the described computational parametric study of nanoparticle focusing using a 3-electrode einzel lens, we draw the following conclusions:

1. The electrostatic focusing in vacuum is described by the non-dimensional focusing parameter χ_e, a ratio of the electrostatic energy to the nominal kinetic energy of the particles entering the focusing region. The average focal length $\langle f_L \rangle$ is seen to have an inverse dependence with χ_e. When confined to about ~20% of the radius of the cylindrical lensing region, the spherical aberration and divergence angle of the particles after crossing the optic axis is minimized, thereby allowing the possibility of realizing tight spot sizes with detailed design. For a specific geometry of the einzel lens, a range of χ_e for which a well-focused particle beam converging at a common focal point is computationally demonstrated. By varying the number of charges on the particles, the particle material (density), size and incoming velocity, it is possible to use the non-dimensional framework introduced here to describe the focusing of aerosol nanoparticles of different sizes and materials as well as einzel lens design.
2. From simulations carried out at finite pressure to probe the effect of particle-gas molecule interactions, a maximum operating pressure above which the einzel lenses ceases to be a useful focusing device is seen to exist. Below the maximum operating pressure (that varies weakly with particle size), the focal length, spherical aberration and divergence angle (after cross over) is seen to vary with χ_e, gas pressure (parameterized by a particle Knudsen number) as well as particle diameter and density (that determines the flow-field local to the particle). Below a certain low pressure, the focusing outcomes are nearly independent of gas

pressure. This will potentially allow the selection of a suitable operating pressure for a 3-electrode einzel lens for a diverse set of particle sizes, materials and focusing voltage.

3. Lastly, we have focused exclusively on parameterizing the effect of the focusing parameter χ_e and the particle initial radial distance (when entering the lens) B_o for simplicity and recognize that in addition to these parameters, the angle distribution of the particle's initial velocity (α_i) and the lens geometry are also important. These parameters need to be probed in future investigations. Further, the focusing relies on particles attaining a high, known charge level to practically obtain targeted values of χ_e. This motivates further work into the charging of sub-100 nm particles to charge levels of ~100, beyond what is currently accomplished (± 3) using ambient bipolar diffusion charging (Gopalakrishnan et al., 2015; Gopalakrishnan et al., 2013). The restriction placed on the spot size due to particle-particle electrostatic repulsion, not considered here, is also a limiting factor to obtain tight spot sizes for nanopatterning, mass-spectrometry or other applications of nanoparticle focusing.

Acknowledgements: This work was partially supported by the DRONES and Data Sciences research grants awarded by the FedEx Institute of Technology, The University of Memphis, and a Faculty Research Grant awarded by the Herff College of Engineering, The University of Memphis.

Table 1: Possible range of χ_e values for different combination of variables

Particle diameter d_p (nm)	**Number of charges n_p**	Initial particle velocity $U_o = 100\ m/s$ and voltage difference $\Delta V = 1000\ V$ Electrostatic focusing parameter $\chi_e = \frac{n_p e \Delta V}{m_p U_o^2}$				
		Gold 19320 kg/m^3	**Silver** 10490 kg/m^3	**Copper 8960** kg/m^3	**Germanium** 5323 kg/m^3	**Silicon** 2330 kg/m^3
100	1	0.0016	0.0029	0.0034	0.0057	0.0131
	100	0.1584	0.2917	0.3415	0.5749	1.3133
	Max (1563)	2.4755	4.5593	5.3378	8.9849	20.5265
50	1	0.0127	0.0233	0.0273	0.0460	0.1051
	100	1.2671	2.3336	2.7321	4.5988	10.5062
	Max (391)	4.9542	9.1244	10.6824	17.9813	41.0793
10	1	1.5838	2.9170	3.4151	5.7485	13.1328
	10	15.8382	29.1700	34.1510	57.4851	131.3276
	Max (16)	25.3411	46.6720	54.6416	91.9762	210.1241
χ_e of an electron is ~ 1.76 - 0.0176, for a potential difference of 1000V, velocity ~10^7 m/s						

Figure 1: A) Schematic representation of the einzel lens geometry (**not to scale**) and the simulation domain considered in this study. B) & C) Schematic representation of the particle trajectories and definitions of influential focusing parameters.

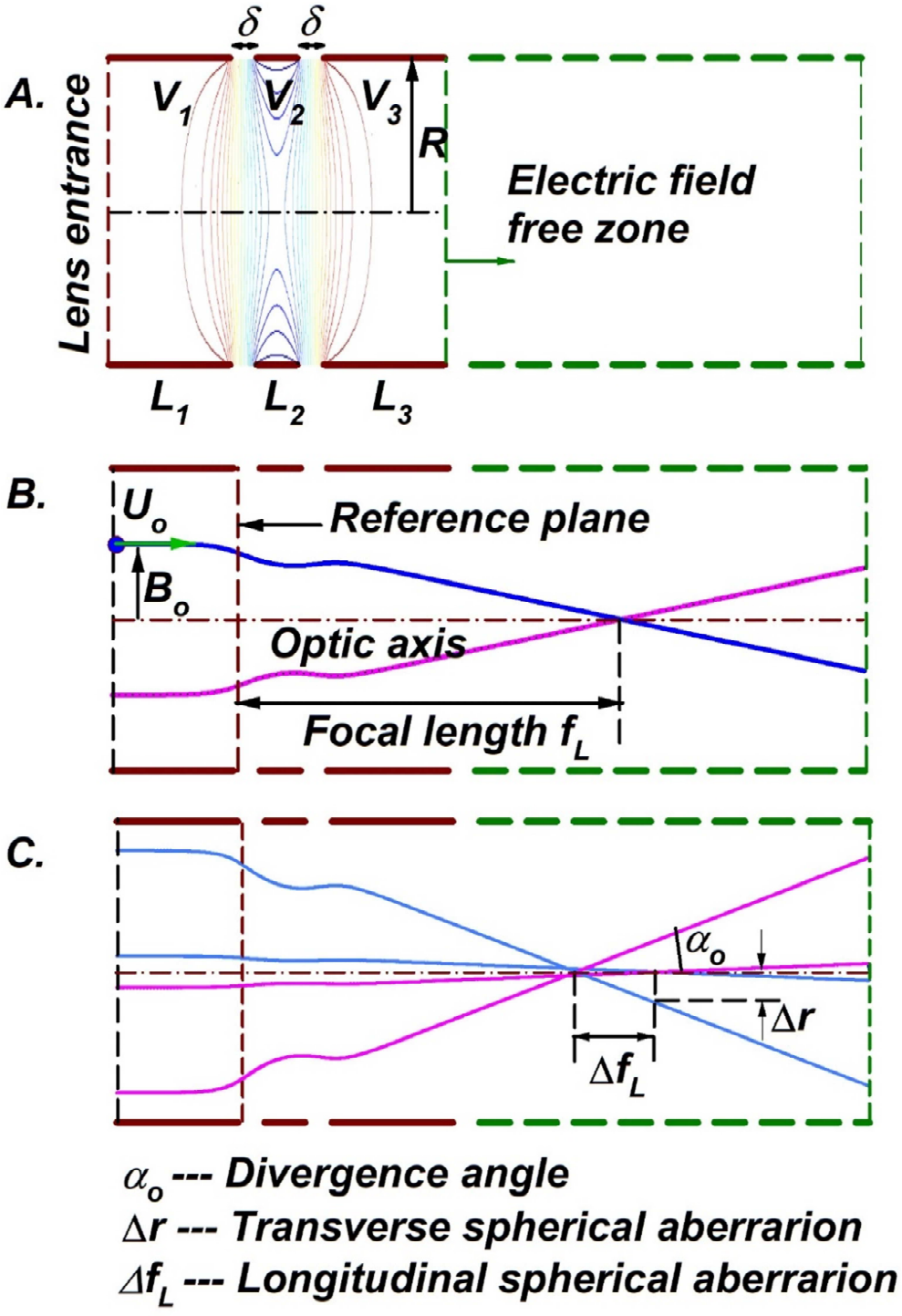

Figure 2: Calculated particle trajectories in vacuum A) $\chi_e = 0.01$ B) $\chi_e = 0.2$ C) $\chi_e = 0.3$ D) $\chi_e = 1$

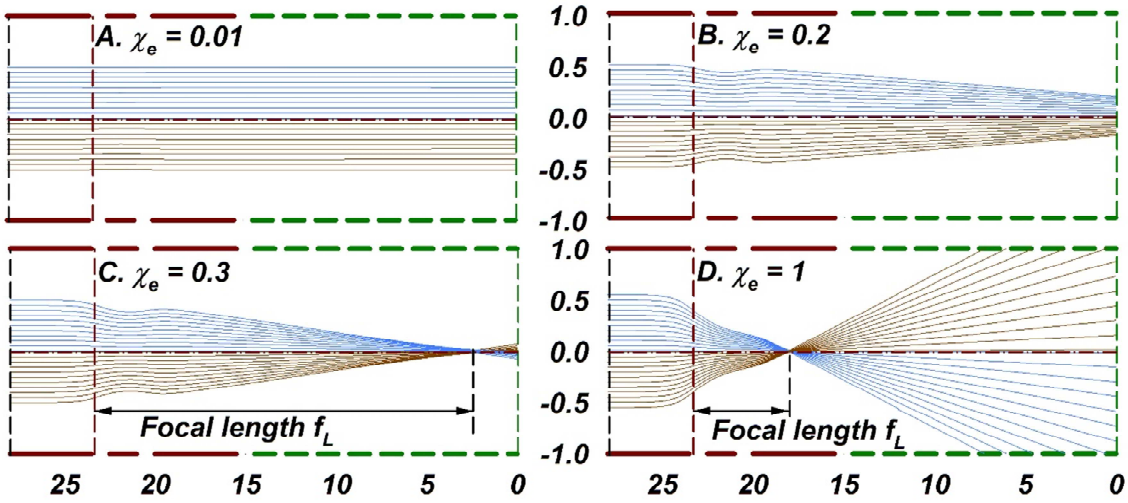

Figure 3: Reproduced with permission from the publisher from Chapter 2.2 ELECTROSTATIC LENSES by K.-J. Hanszen and R. Lauer. **Original caption:** *Particle trajectory and positions of the image side focal and principal points of an electrostatic single lens according to Heise and Rang (1949). The electrical excitation increases from Fig. 2a to Fig. 2d (a, b first operating range, c second range, d third range). ...”*

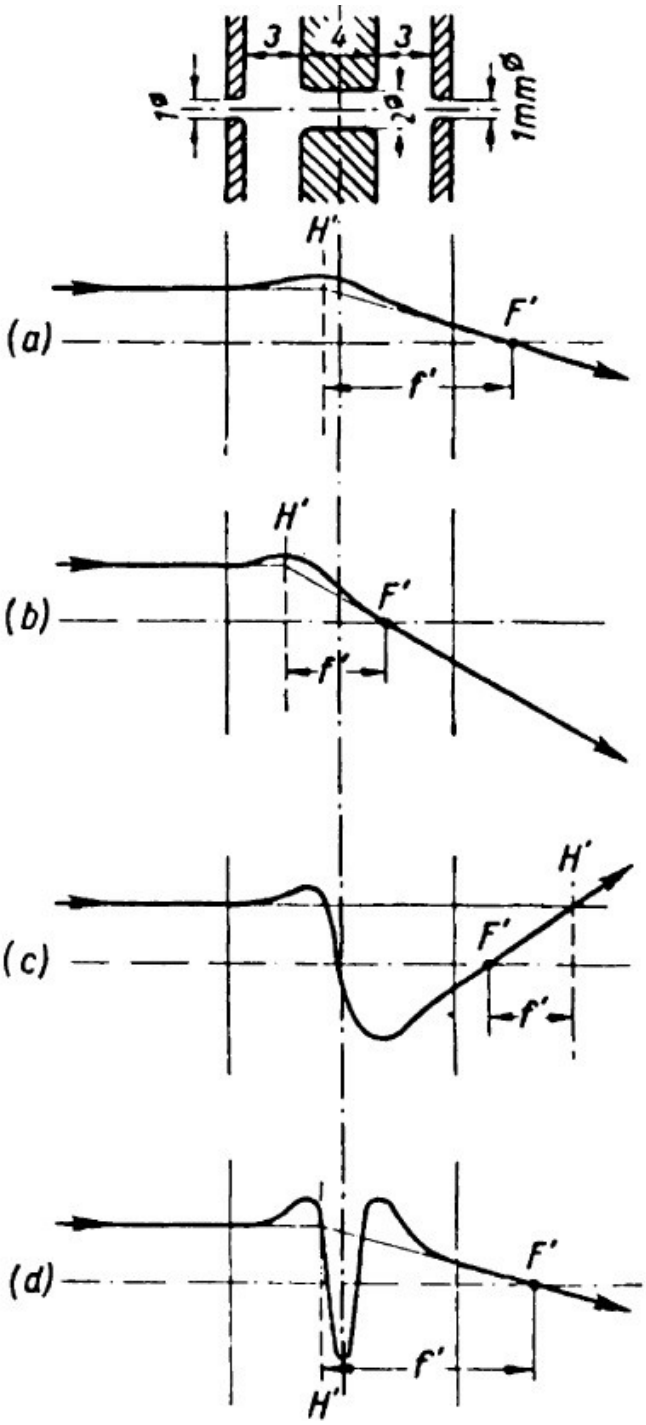

Figure 4: Calculated particle trajectories in vacuum for A) $\chi_e = 3$ B) $\chi_e = 4$ C) $\chi_e = 10$ D) $\chi_e = 275$

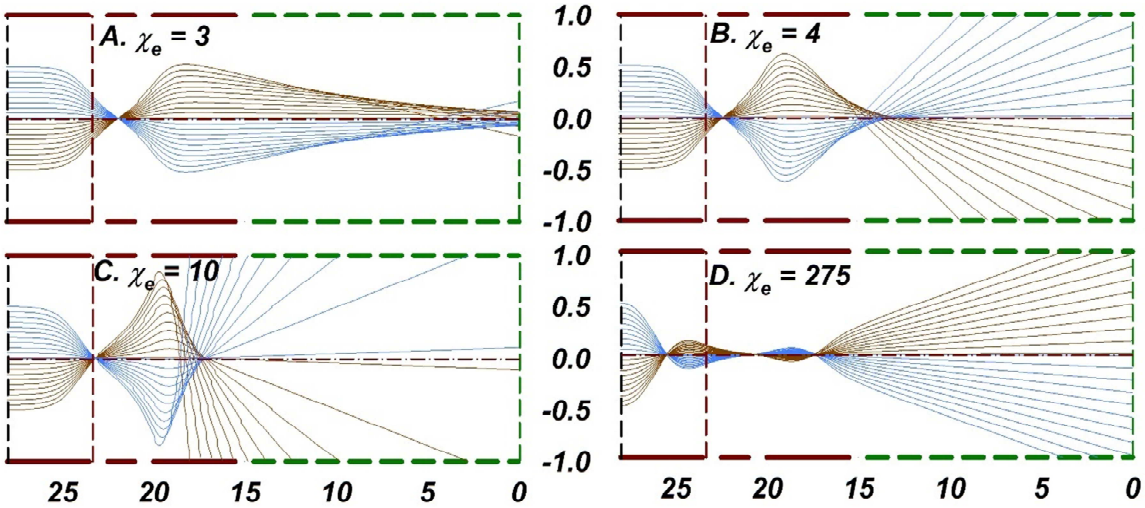

Figure 5: A) Variation of focal length with χ_e. B) Effect of initial radial distance B_o on focal length for various χ_e

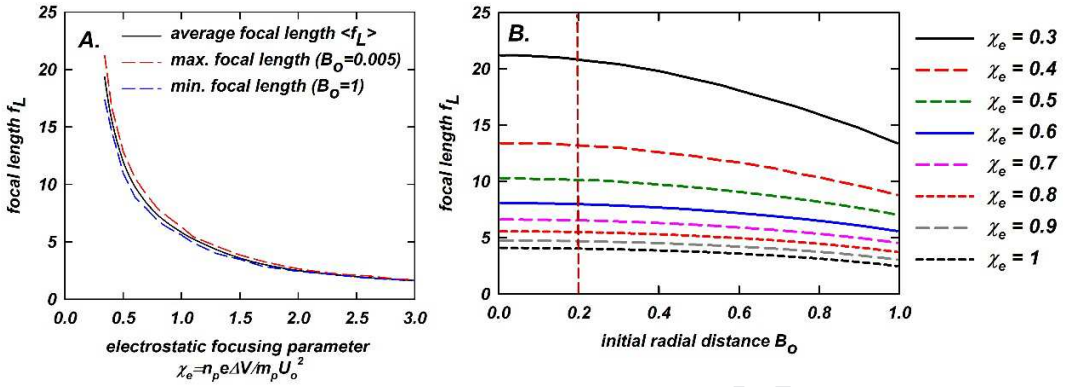

Figure 6: A) Spherical aberration as a function of the initial radial distance B_o for various χ_e. B) The maximum spherical aberration (Δr_{max} corresponding to $B_o = 1$) as a function χ_e. C) Divergence angle as a function of B_o for various χ_e. D) The maximum spherical aberration ($\alpha_{o,max}$ corresponding to $B_o = 1$) as a function χ_e.

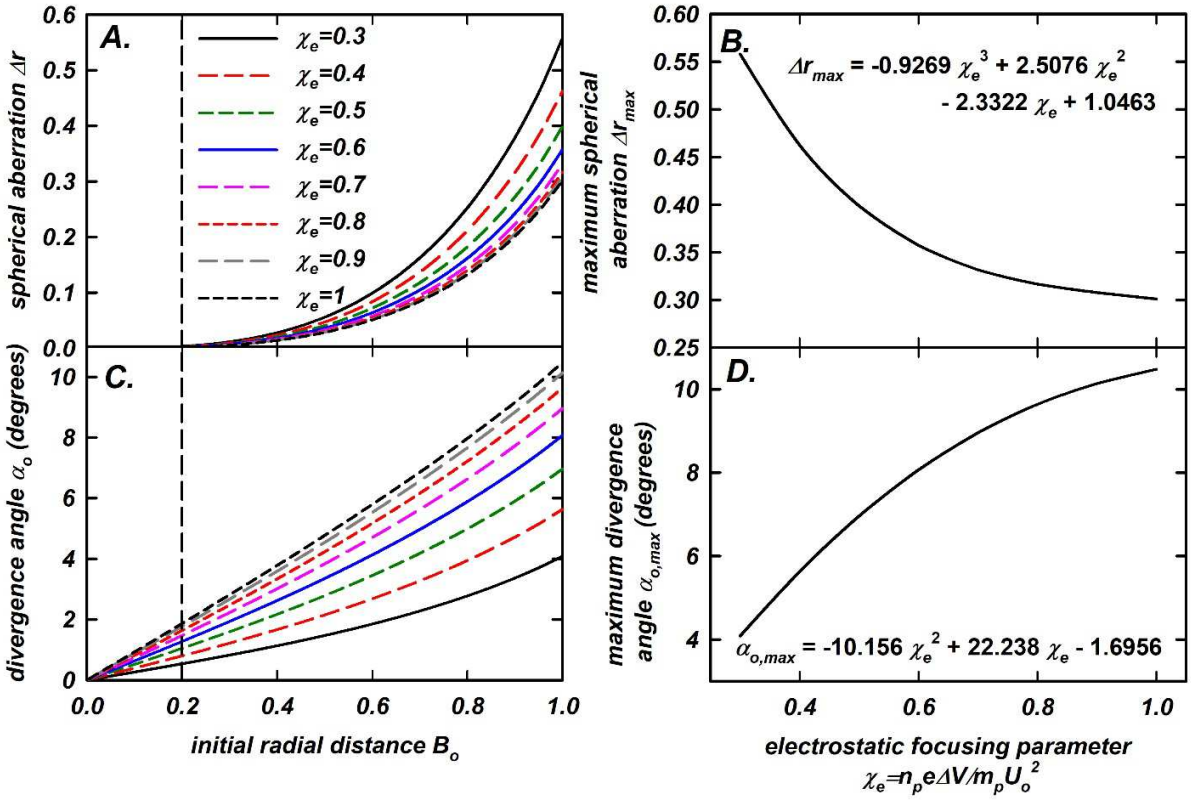

Figure 7: Calculated trajectories of 10 nm gold particles ($\chi_e = 0.3$) at various pressures 0.001 – 100 Pa using Henderson correlation (top panels) and Langevin equation (bottom panels) with pressure noted above each panel.

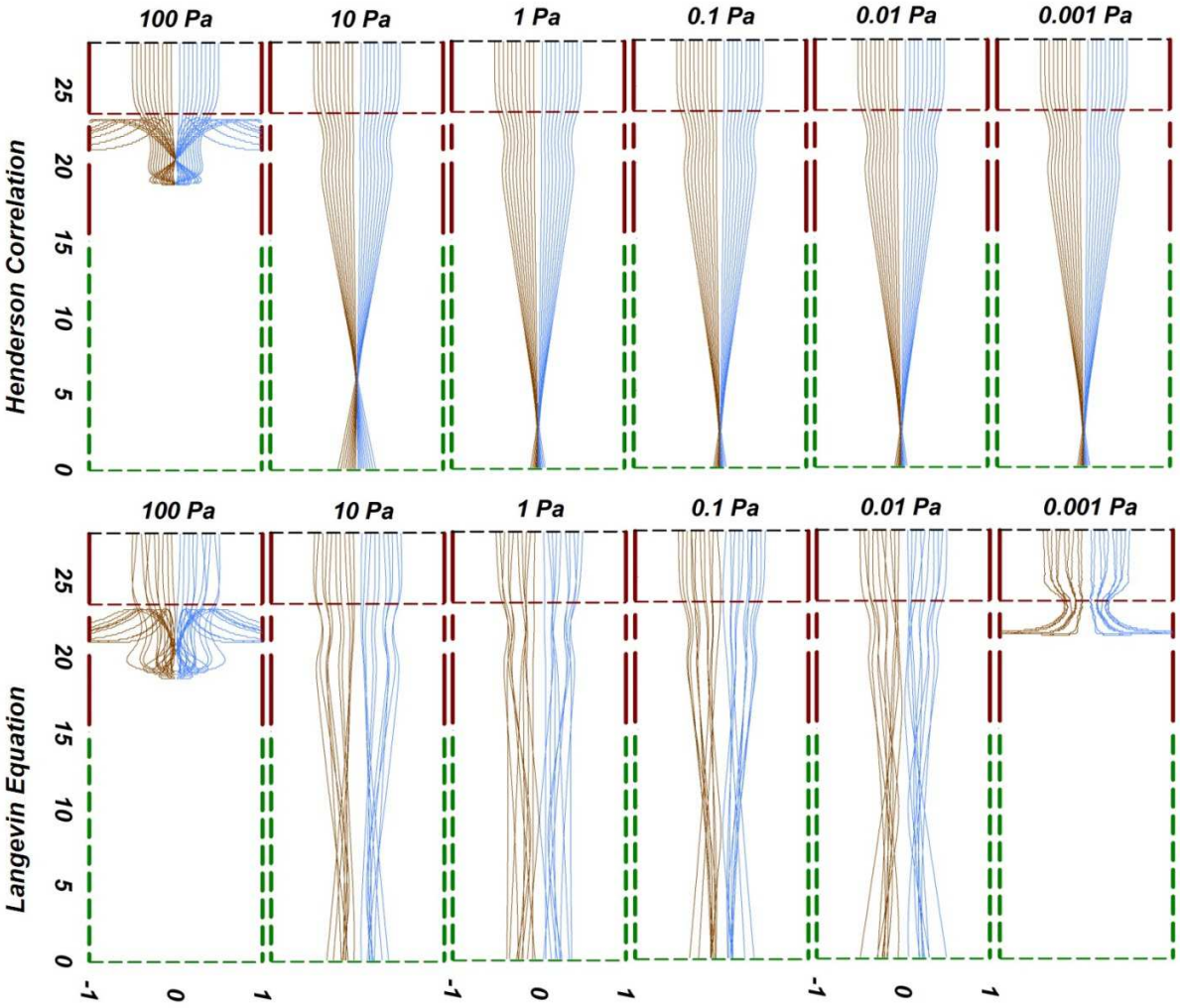

Figure 8: Calculated trajectories of 50 nm gold particles ($\chi_e = 0.3$) at various pressures 0.001 – 200 Pa using Henderson correlation (top panels) and Langevin equation (bottom panels) with pressure noted above each panel.

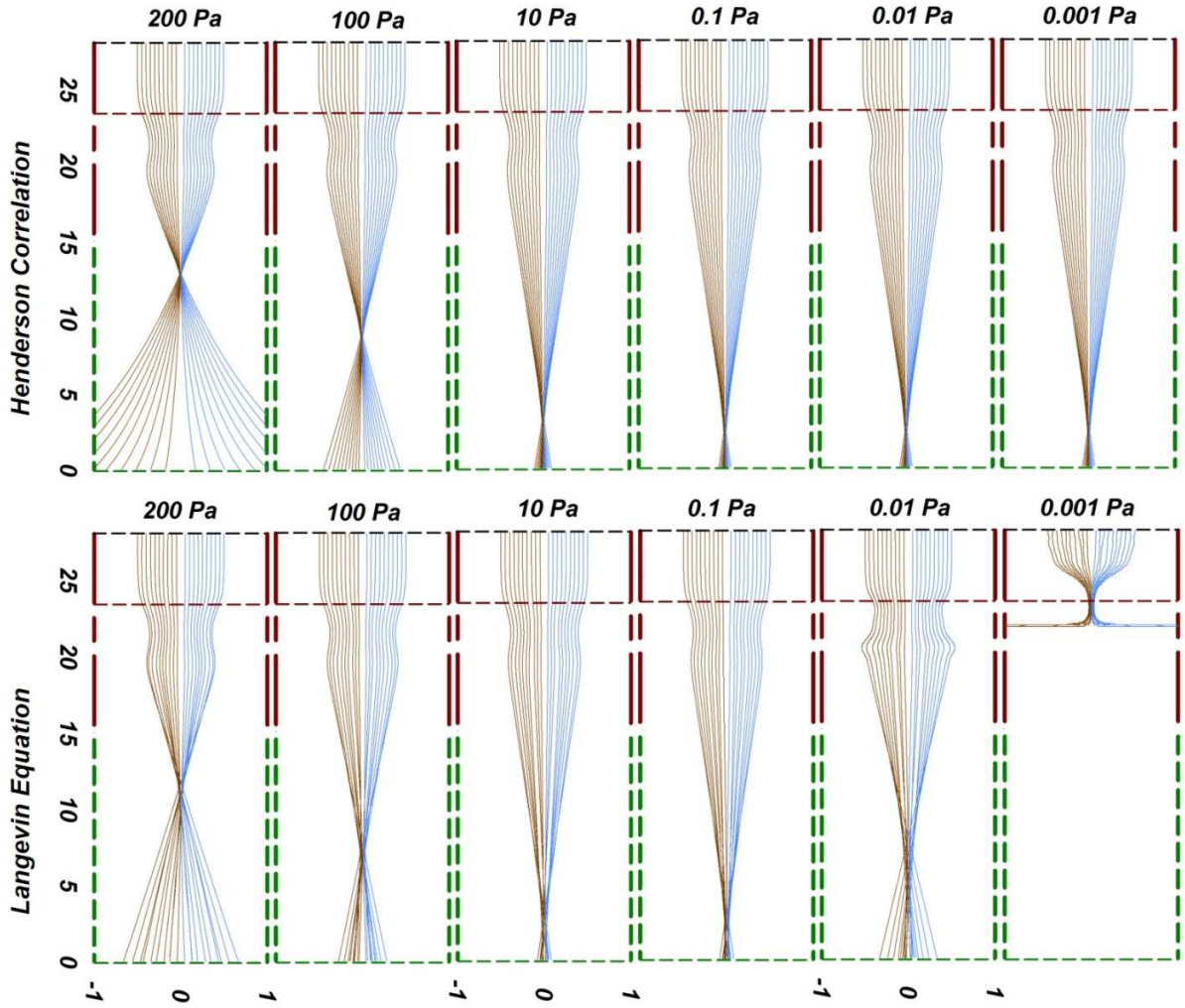

Figure 9: Calculated trajectories of 100 nm gold particles ($\chi_e = 0.3$) at various pressures 0.001 – 400 Pa using Henderson correlation (top panels) and Langevin equation (bottom panels) with pressure noted above each panel. An additional case of trajectories in vacuum is also presented for comparison.

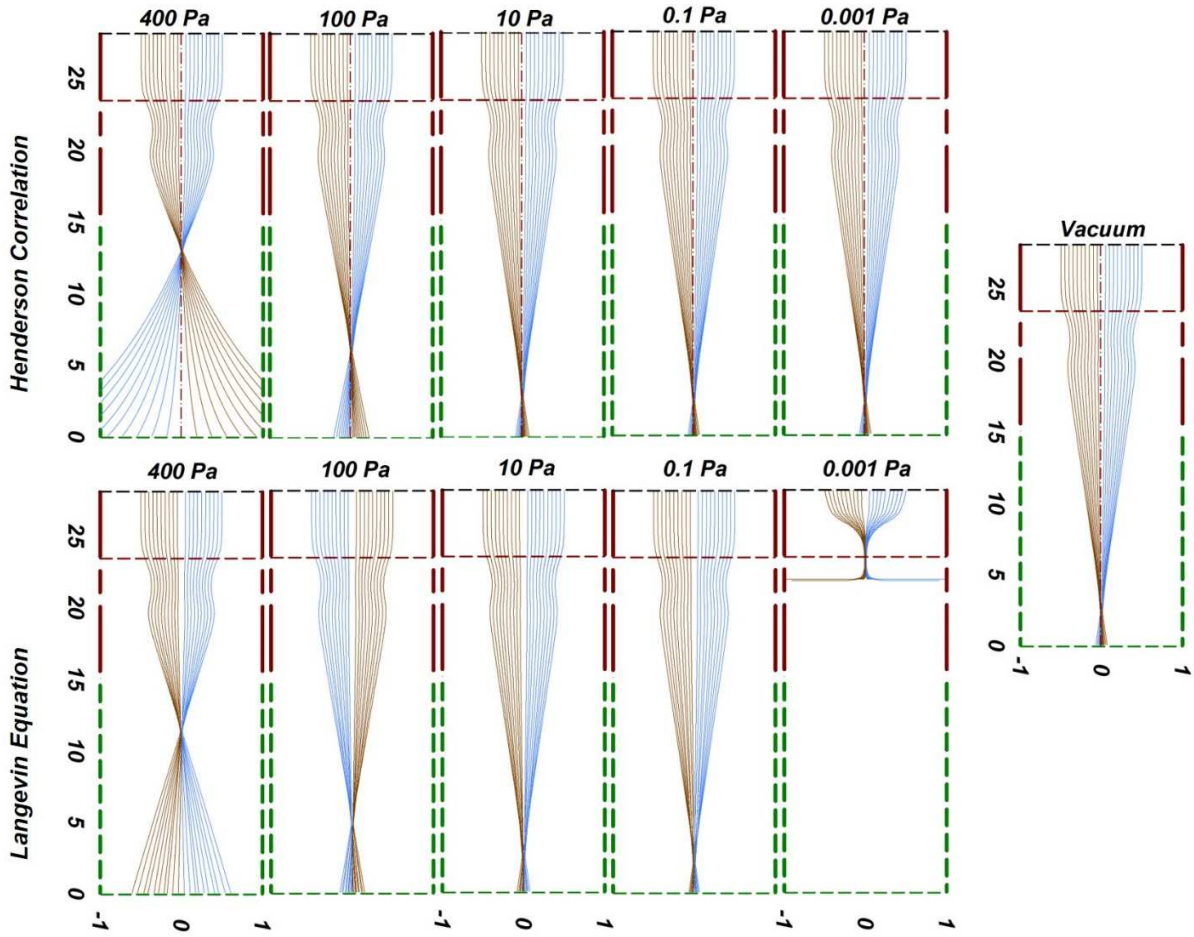

Figure 10: A comparison of the calculated focal length from Henderson's correlation and Langevin equation for different Knudsen number.

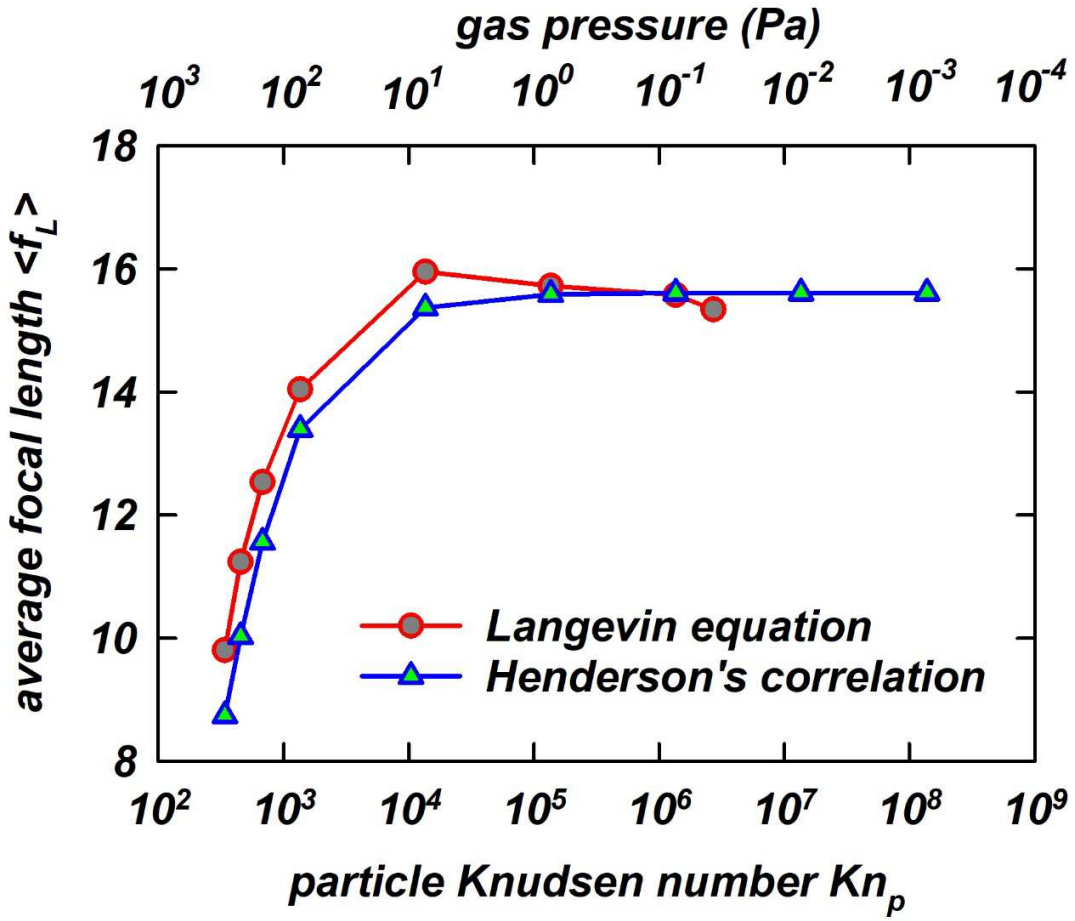

Figure 11: A) Variation of calculated average focal length with particle Knudsen number Kn_p (or gas pressure) for different χ_e. B) A comparison of the variation in average focal length with particle Knudsen number Kn_p (or gas pressure) for particles of different materials and sizes at $\chi_e = 0.4$.

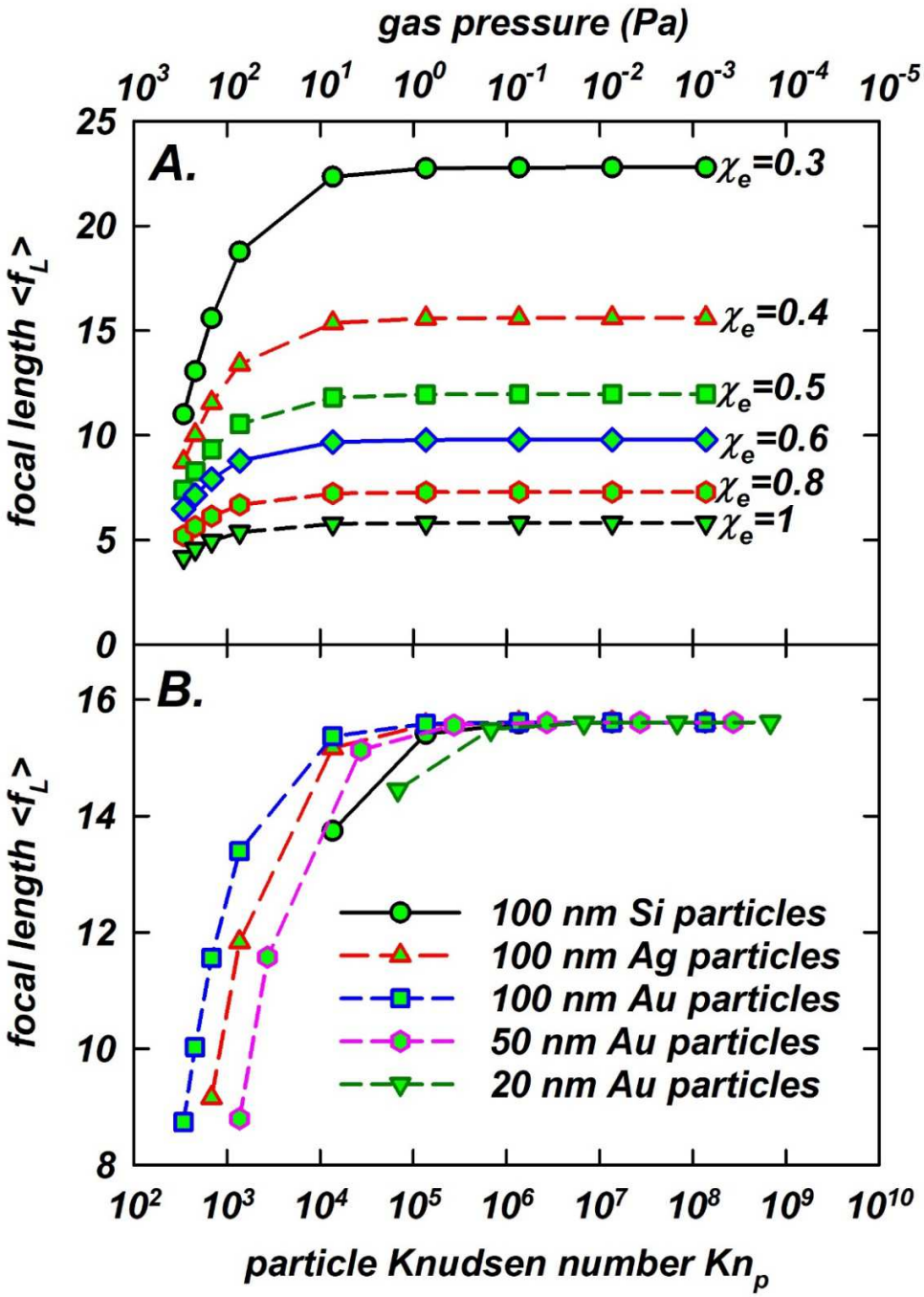

Figure 12: A) Effect of particle Knudsen number Kn_p (or gas pressure) on the maximum spherical aberration for various χ_e. B) Effect of particle Knudsen number Kn_p (or gas pressure) on the maximum divergence angle for various χ_e.

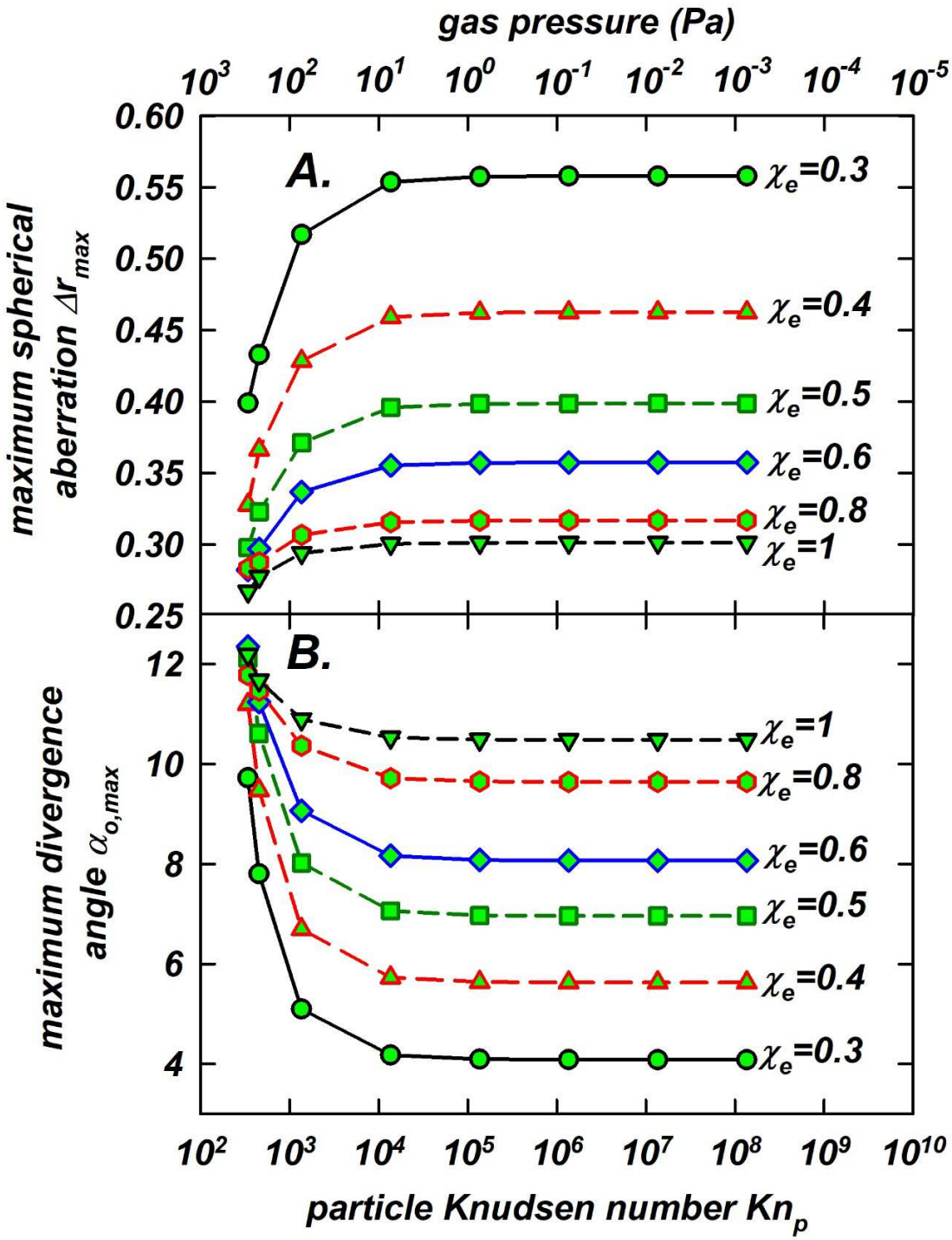

REFERENCES

Abdelsalam, D. G., & Stanislas, M. (2017). Spherical aberration measurement of a microscope objective by use of calibrated spherical particles. *Applied Optics, 56*(16), 4766-4771. doi: 10.1364/AO.56.004766

Adams, A., & Read, F. H. (1972). Electrostatic cylinder lenses II: Three element einzel lenses. *Journal of Physics E: Scientific Instruments, 5*(2), 150-155. doi: 10.1088/0022-3735/5/2/019

Akedo, J., Ichiki, M., Kikuchi, K., & Maeda, R. (1998). Jet molding system for realization of three-dimensional micro-structures. *Sensors and Actuators A: Physical, 69*(1), 106-112. doi: https://doi.org/10.1016/S0924-4247(98)00059-4

Allen, J., & Gould, R. K. (1981). Mass spectrometric analyzer for individual aerosol particles. *Review of Scientific Instruments, 52*(6), 804-809. doi: 10.1063/1.1136700

Chandrasekhar, S. (1943). Stochastic Problems in Physics and Astronomy. *Reviews of Modern Physics, 15*, 1-89.

Chang, T., Thomson, M., Kratschmer, E., Kim, H., Yu, M., Lee, K., Rishton, S., Hussey, B., & Zolgharnain, S. (1996). Electron□beam microcolumns for lithography and related applications. *Journal of Vacuum Science & Technology B: Microelectronics and Nanometer Structures Processing, Measurement, and Phenomena, 14*(6), 3774-3781.

Choi, H., Kang, S., Jung, W., Jung, Y.-h., Park, S. J., Kim, D. S., & Choi, M. (2015). Controlled electrostatic focusing of charged aerosol nanoparticles via an electrified mask. *Journal of Aerosol Science, 88*, 90-97. doi: https://doi.org/10.1016/j.jaerosci.2015.05.017

Ciric, D., Terzic, I., & Vukanic, J. (1976). Symmetrical three-tube unipotential lens. II. First-order focal properties. *Journal of Physics E: Scientific Instruments, 9*(10), 839-847. doi: 10.1088/0022-3735/9/10/017

Cumeras, R., Figueras, E., Davis, C. E., Baumbach, J. I., & Gràcia, I. (2015). Review on ion mobility spectrometry. Part 1: current instrumentation. *The Analyst, 140*(5), 1376-1390. doi: 10.1039/c4an01100g

Dahneke, B., & Cheng, Y. (1979). Properties of continuum source particle beams. I. Calculation methods and results. *Journal of Aerosol Science, 10*(3), 257-274.

Dahneke, B., & Flachsbart, H. (1972). An aerosol beam spectrometer. *Journal of Aerosol Science, 3*(5), 345-349.

Daimon, H., Matsuda, H., Kato, M., & Kudo, M. (2010). Spherical aberration corrected electrostatic lens, input lens, electron spectrometer, photoemission electron microscope and measuring system: Google Patents.

Deng, R., Zhang, X., Smith, K. A., Wormhoudt, J., Lewis, D. K., & Freedman, A. (2008). Focusing particles with diameters of 1 to 10 microns into beams at atmospheric pressure *Aerosol Science and Technology, 42*(11), 899-915. doi: 10.1080/02786820802360674

Di Fonzo, F., Gidwani, A., Fan, M., Neumann, D., Iordanoglou, D., Heberlein, J., McMurry, P., Girshick, S., Tymiak, N., & Gerberich, W. (2000). Focused nanoparticle-beam deposition of patterned microstructures. *Applied Physics Letters, 77*(6), 910-912.

Dong, Y., Bapat, A., Hilchie, S., Kortshagen, U., & Campbell, S. (2004). Generation of nano-sized free standing single crystal silicon particles. *Journal of Vacuum Science & Technology B: Microelectronics and Nanometer Structures Processing, Measurement, and Phenomena, 22*(4), 1923-1930.

Fernández-Maestre, R. (2012). Ion mobility spectrometry: History, characteristics and applications. *Revista U.D.C.A Actualidad & Divulgación Científica, 15*, 467-479.

Fernandez de la Mora, J. (2006). Aerodynamic focusing in spatially periodic flows: Two-dimensional symmetric and antisymmetric channels. *Journal of Aerosol Science, 37*(3), 323-339. doi: http://dx.doi.org/10.1016/j.jaerosci.2005.06.001

Fernandez De La Mora, J., & Riesco-Chueca, P. (2006). Aerodynamic focusing of particles in a carrier gas. *Journal of Fluid Mechanics, 195*, 1-21. doi: 10.1017/S0022112088002307

Gamero-Castaño, M., & Mora, J. F. d. l. (2000). Kinetics of small ion evaporation from the charge and mass distribution of multiply charged clusters in electrosprays. *Journal of Mass Spectrometry, 35*(7), 790-803. doi: https://doi.org/10.1002/1096-9888(200007)35:7<790::AID-JMS21>3.0.CO;2-7

Gopalakrishnan, R., McMurry, P. H., & Hogan, C. J. (2015). The Bipolar Diffusion Charging of Nanoparticles: A Review and Development of Approaches for Non-Spherical Particles. *Aerosol Science and Technology, 49*(12), 1181-1194. doi: 10.1080/02786826.2015.1109053

Gopalakrishnan, R., Meredith, M. J., Larriba-Andaluz, C., & Hogan Jr, C. J. (2013). Brownian dynamics determination of the bipolar steady state charge distribution on spheres and non-spheres in the transition regime. *Journal of Aerosol Science, 63*, 126-145. doi: http://dx.doi.org/10.1016/j.jaerosci.2013.04.007

Hall, T., & Beeman, W. (1976). Secondary electron emission from beams of polystyrene latex spheres. *Journal of Applied Physics, 47*(12), 5222-5225.

Heise, F., & Rang, O. (1949). Experimental investigations of the electrostatic einzel lens. *Optik, 5*, 201-217.

Henderson, C. B. (1976). Drag Coefficients of Spheres in Continuum and Rarefied Flows. *AIAA Journal, 14*(6), 707-708. doi: 10.2514/3.61409

Hinds, W. C. (2012). *Aerosol Technology: Properties, Behavior, and Measurement of Airborne Particles*: Wiley.

Huffman, J. A., Jayne, J. T., Drewnick, F., Aiken, A. C., Onasch, T., Worsnop, D. R., & Jimenez, J. L. (2005). Design, modeling, optimization, and experimental tests of a particle beam width probe for the Aerodyne aerosol mass spectrometer. *Aerosol Science and Technology, 39*(12), 1143-1163. doi: 10.1080/02786820500423782

Hutchins, D. K., Holm, J., & Addison, S. R. (1991). Electrodynamic focusing of charged aerosol particles. *Aerosol Science and Technology, 14*(4), 389-405. doi: 10.1080/02786829108959501

Kane, D. B., Oktem, B., & Johnston, M. V. (2001). An electrostatic lens for focusing charged particles in a mass spectrometer. *Aerosol Science & Technology, 35*(6), 990-997.

Kievit, O., Marijnissen, J. C. M., Verheiljen, P. J. T., & Scarlett, B. (1992). On-line measurement of particle size and composition. *Journal of Aerosol Science, 23*, 301-304. doi: https://doi.org/10.1016/0021-8502(92)90409-O

Kim, H., Kim, J., Yang, H. J., Suh, J., Kim, T., Han, B. W., Kim, S., Kim, D. S., Pikhitsa, P. V., & Choi, M. (2006). Parallel patterning of nanoparticles via electrodynamic focusing of charged aerosols. *Nature Nanotechnology, 1*(2), 117-121. doi: 10.1038/nnano.2006.94

Knutson, E. O., & Whitby, K. T. (1975). Aerosol classification by electric mobility: apparatus, theory, and applications. *Journal of Aerosol Science, 6*(6), 443-451. doi: http://dx.doi.org/10.1016/0021-8502(75)90060-9

Krinke, T. J., Deppert, K., Magnusson, M. H., Schmidt, F., & Fissan, H. (2002). Microscopic aspects of the deposition of nanoparticles from the gas phase. *Journal of Aerosol Science, 33*(10), 1341-1359. doi: https://doi.org/10.1016/S0021-8502(02)00074-5

Langevin, P. (1903). *Ann. Chim. Phys., 28*, 289.

Lee, K.-S., Cho, S.-W., & Lee, D. (2008). Development and experimental evaluation of aerodynamic lens as an aerosol inlet of single particle mass spectrometry. *Journal of Aerosol Science, 39*(4), 287-304. doi: https://doi.org/10.1016/j.jaerosci.2007.10.011

Lee, K.-S., Hwang, T.-H., Kim, S.-H., Kim, S. H., & Lee, D. (2013). Numerical simulations on aerodynamic focusing of particles in a wide size range of 30 nm–10 μm. *Aerosol Science and Technology, 47*(9), 1001-1008. doi: 10.1080/02786826.2013.808737

Lee, K.-S., Kim, S., & Lee, D. (2009). Aerodynamic focusing of 5–50nm nanoparticles in air. *Journal of Aerosol Science, 40*(12), 1010-1018. doi: https://doi.org/10.1016/j.jaerosci.2009.09.004

Lin, E.-C., Cole, J. J., & Jacobs, H. O. (2010). Gas phase electrodeposition: A programmable multimaterial deposition method for combinatorial nanostructured device discovery. *Nano Letters, 10*(11), 4494-4500. doi: 10.1021/nl102344r

Liu, P., Ziemann, P. J., Kittelson, D. B., & McMurry, P. H. (1995a). Generating Particle Beams of Controlled Dimensions and Divergence .1. Experimental Evaluation of Particle Motion in Aerodynamic Lenses and Nozzle Expansions. *Aerosol Science and Technology, 22*(3), 293-313. doi: 10.1080/02786829408959748

Liu, P., Ziemann, P. J., Kittelson, D. B., & McMurry, P. H. (1995b). Generating Particle Beams of Controlled Dimensions and Divergence .2. Experimental Evaluation of Particle Motion in Aerodynamic Lenses and Nozzle Expansions. *Aerosol Science and Technology, 22*(3), 314-324. doi: 10.1080/02786829408959749

Masuda, S., Fujibayashi, K., Ishida, K., & Inaba, H. (1972). Confinement and transportation of charged aerosol clouds via electric curtain. *Electrical Engineering in Japan, 92*(1), 43-52. doi: doi:10.1002/eej.4390920106

Matsui, H., Ichihashi, M., Ueda, S., Otaka, T., Takahashi, K., Kobari, T., & Odaka, K. (1995). Charged particle beam apparatus including means for maintaining a vacuum seal: Google Patents.

Mazur, P., & Oppenheim, I. (1970). Molecular theory of brownian motion. *Physica, 50*(2), 241-258. doi: 10.1016/0031-8914(70)90005-4

Murphy, W. K., & Sears, G. W. (1964). Production of particulate beams. *Journal of Applied Physics, 35*(6), 1986-1987. doi: 10.1063/1.1713788

Oberreit, D. R., & Hogan Jr, C. J. (2015). Drift tube ion mobility spectrometer for aerosol measurement: Google Patents.

Odenthal, C. J. (1991). Pinched electron beam cathode-ray tube with high-voltage einzel focus lens: Google Patents.

Park, J., Jeong, J., Kim, C., & Hwang, J. (2013). Deposition of Charged Aerosol Particles on a Substrate by Collimating Through an Electric Field Assisted Coaxial Flow Nozzle. *Aerosol Science and Technology, 47*(5), 512-519. doi: 10.1080/02786826.2013.767981

Qi, L., McMurry, P. H., Norris, D. J., & Girshick, S. L. (2010). Micropattern deposition of colloidal semiconductor nanocrystals by aerodynamic focusing. *Aerosol Science and Technology, 44*(1), 55-60. doi: 10.1080/02786820903376876

Robinson, A. (1956). On the motion of small particles in a potential field of flow. *Communications on Pure and Applied Mathematics, 9*(1), 69-84. doi: doi:10.1002/cpa.3160090105

Rusinque, H., Fedianina, E., Weber, A., & Brenner, G. (2019). Numerical study of the controlled electrodeposition of charged nanoparticles in an electric field. *Journal of Aerosol Science, 129*, 28-39. doi: https://doi.org/10.1016/j.jaerosci.2018.11.005

Schreiner, J., Schild, U., Voigt, C., & Mauersberger, K. (1999). Focusing of aerosols into a particle beam at pressures from 10 to 150 Torr *Aerosol Science and Technology, 31*(5), 373-382. doi: 10.1080/027868299304093

Schreiner, J., Voigt, C., Mauersberger, K., McMurry, P., & Ziemann, P. (1998). Aerodynamic lens system for producing particle beams at stratospheric pressures. *Aerosol Science and Technology, 29*(1), 50-56. doi: 10.1080/02786829808965550

Seapan, M., Selman, D., Seale, F., Siebers, G., & Wissler, E. H. (1982). Aerosol characterization using molecular beam techniques. *Journal of Colloid and Interface Science, 87*(1), 154-166. doi: https://doi.org/10.1016/0021-9797(82)90379-4

Sinha, M. P., & Friedlander, S. K. (1986). Mass distribution of chemical species in a polydisperse aerosol: Measurement of sodium chloride in particles by mass spectrometry. *Journal of Colloid and Interface Science, 112*(2), 573-582. doi: https://doi.org/10.1016/0021-9797(86)90128-1

Thomson, B. A., & Iribarne, J. V. (1979). Field induced ion evaporation from liquid surfaces at atmospheric pressure. *The Journal of Chemical Physics, 71*(11), 4451-4463. doi: 10.1063/1.438198

Tse, L., & Barton, K. (2015). Airflow assisted printhead for high-resolution electrohydrodynamic jet printing onto non-conductive and tilted surfaces. *Applied Physics Letters, 107*(5), 054103. doi: 10.1063/1.4928482

Verlet, L. (1967). Computer "experiments" on classical fluids. I. Thermodynamical properties of Lennard-Jones molecules. *Physical Review, 159*(1), 98-103.

Wang, X., Kruis, F. E., & McMurry, P. H. (2005). Aerodynamic Focusing of Nanoparticles: I. Guidelines for Designing Aerodynamic Lenses for Nanoparticles. *Aerosol Science and Technology, 39*(7), 611-623. doi: 10.1080/02786820500181901

Weißbäcker, C., & Rose, H. (2001). Electrostatic correction of the chromatic and of the spherical aberration of charged□particle lenses. *Journal of Electron Microscopy, 50*(5), 383-390. doi: 10.1093/jmicro/50.5.383

You, S., & Choi, M. (2007). Numerical simulation of microscopic motion and deposition of nanoparticles via electrodynamic focusing. *Journal of Aerosol Science, 38*(11), 1140-1149. doi: https://doi.org/10.1016/j.jaerosci.2007.08.002

You, S., Han, K., Kim, H., Lee, H., Woo, C. G., Jeong, C., Nam, W., & Choi, M. (2010). Nanoparticle patterning: High-resolution, parallel patterning of nanoparticles via an ion-induced focusing mask. *Small, 6*(19). doi: 10.1002/smll.201090063

Zhang, X., Smith, K. A., Worsnop, D. R., Jimenez, J. L., Jayne, J. T., Kolb, C. E., Morris, J., & Davidovits, P. (2004). Numerical characterization of particle beam collimation: Part II

Integrated aerodynamic-lens–nozzle system. *Aerosol Science and Technology, 38*(6), 619-638. doi: 10.1080/02786820490479833

ELSEVIER LICENSE
TERMS AND CONDITIONS

Apr 12, 2019

This Agreement between THE UNIVERSITY OF MEMPHIS -- RANGANATHAN GOPALAKRISHNAN ("You") and Elsevier ("Elsevier") consists of your license details and the terms and conditions provided by Elsevier and Copyright Clearance Center.

License Number	4566060947123
License date	Apr 11, 2019
Licensed Content Publisher	Elsevier
Licensed Content Publication	Elsevier Books
Licensed Content Title	Focusing of Charged Particles
Licensed Content Author	K.-J. Hanszen,R. Lauer
Licensed Content Date	Jan 1, 1967
Licensed Content Pages	57
Start Page	251
End Page	307
Type of Use	reuse in a journal/magazine
Requestor type	academic/educational institute
Intended publisher of new work	Elsevier
Portion	figures/tables/illustrations
Number of figures/tables/illustrations	1
Format	both print and electronic
Are you the author of this Elsevier chapter?	No
Will you be translating?	No
Original figure numbers	figure 2 in "CHAPTER 2.2 - ELECTROSTATIC LENSES".
Title of the article	Computational study of electrostatic focusing of aerosol nanoparticles using a 3-electrode Einzel lens
Publication new article is in	Journal of Aerosol Science
Publisher of the new article	Elsevier
Author of new article	Rayhan Ahmed and Ranganathan Gopalakrishnan
Expected publication date	Oct 2019
Estimated size of new article (number of pages)	10
Requestor Location	THE UNIVERSITY OF MEMPHIS 312 Engineering Science The University of Memphis MEMPHIS, TN 38152 United States Attn: THE UNIVERSITY OF MEMPHIS

Publisher Tax ID	98-0397604
Total	0.00 USD

Terms and Conditions

INTRODUCTION

1. The publisher for this copyrighted material is Elsevier. By clicking "accept" in connection with completing this licensing transaction, you agree that the following terms and conditions apply to this transaction (along with the Billing and Payment terms and conditions established by Copyright Clearance Center, Inc. ("CCC"), at the time that you opened your Rightslink account and that are available at any time at http://myaccount.copyright.com).

GENERAL TERMS

2. Elsevier hereby grants you permission to reproduce the aforementioned material subject to the terms and conditions indicated.
3. Acknowledgement: If any part of the material to be used (for example, figures) has appeared in our publication with credit or acknowledgement to another source, permission must also be sought from that source. If such permission is not obtained then that material may not be included in your publication/copies. Suitable acknowledgement to the source must be made, either as a footnote or in a reference list at the end of your publication, as follows:
"Reprinted from Publication title, Vol /edition number, Author(s), Title of article / title of chapter, Pages No., Copyright (Year), with permission from Elsevier [OR APPLICABLE SOCIETY COPYRIGHT OWNER]." Also Lancet special credit - "Reprinted from The Lancet, Vol. number, Author(s), Title of article, Pages No., Copyright (Year), with permission from Elsevier."
4. Reproduction of this material is confined to the purpose and/or media for which permission is hereby given.
5. Altering/Modifying Material: Not Permitted. However figures and illustrations may be altered/adapted minimally to serve your work. Any other abbreviations, additions, deletions and/or any other alterations shall be made only with prior written authorization of Elsevier Ltd. (Please contact Elsevier at permissions@elsevier.com). No modifications can be made to any Lancet figures/tables and they must be reproduced in full.
6. If the permission fee for the requested use of our material is waived in this instance, please be advised that your future requests for Elsevier materials may attract a fee.
7. Reservation of Rights: Publisher reserves all rights not specifically granted in the combination of (i) the license details provided by you and accepted in the course of this licensing transaction, (ii) these terms and conditions and (iii) CCC's Billing and Payment terms and conditions.
8. License Contingent Upon Payment: While you may exercise the rights licensed immediately upon issuance of the license at the end of the licensing process for the transaction, provided that you have disclosed complete and accurate details of your proposed use, no license is finally effective unless and until full payment is received from you (either by publisher or by CCC) as provided in CCC's Billing and Payment terms and conditions. If full payment is not received on a timely basis, then any license preliminarily granted shall be deemed automatically revoked and shall be void as if never granted. Further, in the event that you breach any of these terms and conditions or any of CCC's Billing and Payment terms and conditions, the license is automatically revoked and shall be void as if never granted. Use of materials as described in a revoked license, as well as any use of the materials beyond the scope of an unrevoked license, may constitute copyright infringement and publisher reserves the right to take any and all action to protect its copyright in the materials.
9. Warranties: Publisher makes no representations or warranties with respect to the licensed material.
10. Indemnity: You hereby indemnify and agree to hold harmless publisher and CCC, and their respective officers, directors, employees and agents, from and against any and all

claims arising out of your use of the licensed material other than as specifically authorized pursuant to this license.
11. No Transfer of License: This license is personal to you and may not be sublicensed, assigned, or transferred by you to any other person without publisher's written permission.
12. No Amendment Except in Writing: This license may not be amended except in a writing signed by both parties (or, in the case of publisher, by CCC on publisher's behalf).
13. Objection to Contrary Terms: Publisher hereby objects to any terms contained in any purchase order, acknowledgment, check endorsement or other writing prepared by you, which terms are inconsistent with these terms and conditions or CCC's Billing and Payment terms and conditions. These terms and conditions, together with CCC's Billing and Payment terms and conditions (which are incorporated herein), comprise the entire agreement between you and publisher (and CCC) concerning this licensing transaction. In the event of any conflict between your obligations established by these terms and conditions and those established by CCC's Billing and Payment terms and conditions, these terms and conditions shall control.
14. Revocation: Elsevier or Copyright Clearance Center may deny the permissions described in this License at their sole discretion, for any reason or no reason, with a full refund payable to you. Notice of such denial will be made using the contact information provided by you. Failure to receive such notice will not alter or invalidate the denial. In no event will Elsevier or Copyright Clearance Center be responsible or liable for any costs, expenses or damage incurred by you as a result of a denial of your permission request, other than a refund of the amount(s) paid by you to Elsevier and/or Copyright Clearance Center for denied permissions.

LIMITED LICENSE

The following terms and conditions apply only to specific license types:
15. **Translation**: This permission is granted for non-exclusive world **English** rights only unless your license was granted for translation rights. If you licensed translation rights you may only translate this content into the languages you requested. A professional translator must perform all translations and reproduce the content word for word preserving the integrity of the article.
16. **Posting licensed content on any Website**: The following terms and conditions apply as follows: Licensing material from an Elsevier journal: All content posted to the web site must maintain the copyright information line on the bottom of each image; A hyper-text must be included to the Homepage of the journal from which you are licensing at http://www.sciencedirect.com/science/journal/xxxxx or the Elsevier homepage for books at http://www.elsevier.com; Central Storage: This license does not include permission for a scanned version of the material to be stored in a central repository such as that provided by Heron/XanEdu.
Licensing material from an Elsevier book: A hyper-text link must be included to the Elsevier homepage at http://www.elsevier.com . All content posted to the web site must maintain the copyright information line on the bottom of each image.

Posting licensed content on Electronic reserve: In addition to the above the following clauses are applicable: The web site must be password-protected and made available only to bona fide students registered on a relevant course. This permission is granted for 1 year only. You may obtain a new license for future website posting.
17. **For journal authors:** the following clauses are applicable in addition to the above:
Preprints:
A preprint is an author's own write-up of research results and analysis, it has not been peer-reviewed, nor has it had any other value added to it by a publisher (such as formatting, copyright, technical enhancement etc.).
Authors can share their preprints anywhere at any time. Preprints should not be added to or enhanced in any way in order to appear more like, or to substitute for, the final versions of

articles however authors can update their preprints on arXiv or RePEc with their Accepted Author Manuscript (see below).
If accepted for publication, we encourage authors to link from the preprint to their formal publication via its DOI. Millions of researchers have access to the formal publications on ScienceDirect, and so links will help users to find, access, cite and use the best available version. Please note that Cell Press, The Lancet and some society-owned have different preprint policies. Information on these policies is available on the journal homepage.
Accepted Author Manuscripts: An accepted author manuscript is the manuscript of an article that has been accepted for publication and which typically includes author-incorporated changes suggested during submission, peer review and editor-author communications.
Authors can share their accepted author manuscript:

- immediately
  - via their non-commercial person homepage or blog
  - by updating a preprint in arXiv or RePEc with the accepted manuscript
  - via their research institute or institutional repository for internal institutional uses or as part of an invitation-only research collaboration work-group
  - directly by providing copies to their students or to research collaborators for their personal use
  - for private scholarly sharing as part of an invitation-only work group on commercial sites with which Elsevier has an agreement
- After the embargo period
  - via non-commercial hosting platforms such as their institutional repository
  - via commercial sites with which Elsevier has an agreement

In all cases accepted manuscripts should:

- link to the formal publication via its DOI
- bear a CC-BY-NC-ND license - this is easy to do
- if aggregated with other manuscripts, for example in a repository or other site, be shared in alignment with our hosting policy not be added to or enhanced in any way to appear more like, or to substitute for, the published journal article.

Published journal article (JPA): A published journal article (PJA) is the definitive final record of published research that appears or will appear in the journal and embodies all value-adding publishing activities including peer review co-ordination, copy-editing, formatting, (if relevant) pagination and online enrichment.
Policies for sharing publishing journal articles differ for subscription and gold open access articles:
Subscription Articles: If you are an author, please share a link to your article rather than the full-text. Millions of researchers have access to the formal publications on ScienceDirect, and so links will help your users to find, access, cite, and use the best available version.
Theses and dissertations which contain embedded PJAs as part of the formal submission can be posted publicly by the awarding institution with DOI links back to the formal publications on ScienceDirect.
If you are affiliated with a library that subscribes to ScienceDirect you have additional private sharing rights for others' research accessed under that agreement. This includes use for classroom teaching and internal training at the institution (including use in course packs and courseware programs), and inclusion of the article for grant funding purposes.
Gold Open Access Articles: May be shared according to the author-selected end-user license and should contain a CrossMark logo, the end user license, and a DOI link to the formal publication on ScienceDirect.
Please refer to Elsevier's posting policy for further information.

18. **For book authors** the following clauses are applicable in addition to the above: Authors are permitted to place a brief summary of their work online only. You are not allowed to download and post the published electronic version of your chapter, nor may you scan the printed edition to create an electronic version. **Posting to a repository:** Authors are permitted to post a summary of their chapter only in their institution's repository.
19. **Thesis/Dissertation**: If your license is for use in a thesis/dissertation your thesis may be submitted to your institution in either print or electronic form. Should your thesis be published commercially, please reapply for permission. These requirements include permission for the Library and Archives of Canada to supply single copies, on demand, of the complete thesis and include permission for Proquest/UMI to supply single copies, on demand, of the complete thesis. Should your thesis be published commercially, please reapply for permission. Theses and dissertations which contain embedded PJAs as part of the formal submission can be posted publicly by the awarding institution with DOI links back to the formal publications on ScienceDirect.

Elsevier Open Access Terms and Conditions

You can publish open access with Elsevier in hundreds of open access journals or in nearly 2000 established subscription journals that support open access publishing. Permitted third party re-use of these open access articles is defined by the author's choice of Creative Commons user license. See our open access license policy for more information.

Terms & Conditions applicable to all Open Access articles published with Elsevier:

Any reuse of the article must not represent the author as endorsing the adaptation of the article nor should the article be modified in such a way as to damage the author's honour or reputation. If any changes have been made, such changes must be clearly indicated.

The author(s) must be appropriately credited and we ask that you include the end user license and a DOI link to the formal publication on ScienceDirect.

If any part of the material to be used (for example, figures) has appeared in our publication with credit or acknowledgement to another source it is the responsibility of the user to ensure their reuse complies with the terms and conditions determined by the rights holder.

Additional Terms & Conditions applicable to each Creative Commons user license:

CC BY: The CC-BY license allows users to copy, to create extracts, abstracts and new works from the Article, to alter and revise the Article and to make commercial use of the Article (including reuse and/or resale of the Article by commercial entities), provided the user gives appropriate credit (with a link to the formal publication through the relevant DOI), provides a link to the license, indicates if changes were made and the licensor is not represented as endorsing the use made of the work. The full details of the license are available at http://creativecommons.org/licenses/by/4.0.

CC BY NC SA: The CC BY-NC-SA license allows users to copy, to create extracts, abstracts and new works from the Article, to alter and revise the Article, provided this is not done for commercial purposes, and that the user gives appropriate credit (with a link to the formal publication through the relevant DOI), provides a link to the license, indicates if changes were made and the licensor is not represented as endorsing the use made of the work. Further, any new works must be made available on the same conditions. The full details of the license are available at http://creativecommons.org/licenses/by-nc-sa/4.0.

CC BY NC ND: The CC BY-NC-ND license allows users to copy and distribute the Article, provided this is not done for commercial purposes and further does not permit distribution of the Article if it is changed or edited in any way, and provided the user gives appropriate credit (with a link to the formal publication through the relevant DOI), provides a link to the license, and that the licensor is not represented as endorsing the use made of the work. The full details of the license are available at http://creativecommons.org/licenses/by-nc-nd/4.0.

Any commercial reuse of Open Access articles published with a CC BY NC SA or CC BY NC ND license requires permission from Elsevier and will be subject to a fee.

Commercial reuse includes:

- Associating advertising with the full text of the Article
- Charging fees for document delivery or access
- Article aggregation
- Systematic distribution via e-mail lists or share buttons

Posting or linking by commercial companies for use by customers of those companies.

20. **Other Conditions**:

v1.9

Questions? customercare@copyright.com or +1-855-239-3415 (toll free in the US) or +1-978-646-2777.

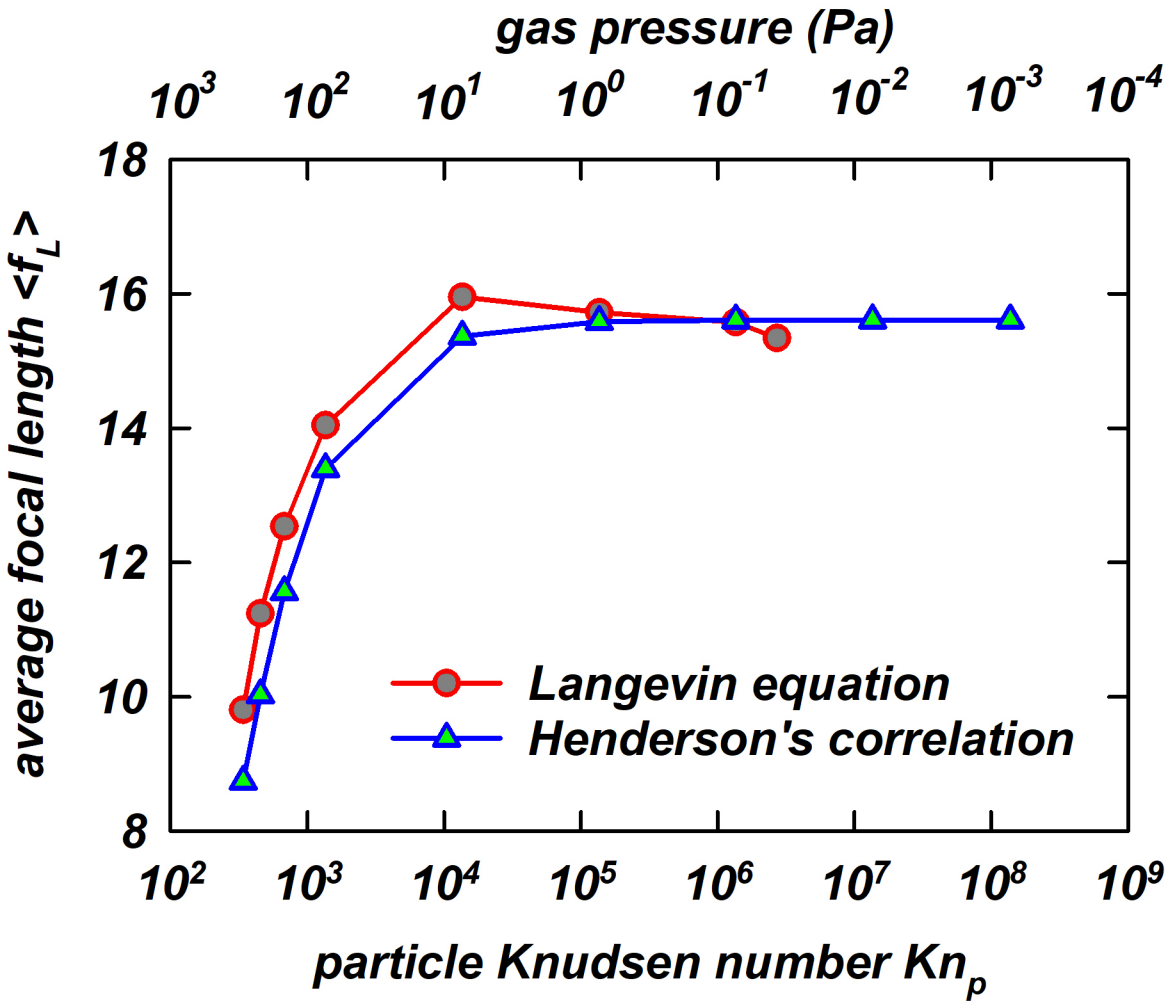
gas pressure (Pa)
10^3
10^2
10^1
10^0
10^-1
10^-2
10^-3
10^-4
18
16
14
12
10
8
average focal length <f_L>
Langevin equation
Henderson's correlation
10^2
10^3
10^4
10^5
10^6
10^7
10^8
10^9
particle Knudsen number Kn_p

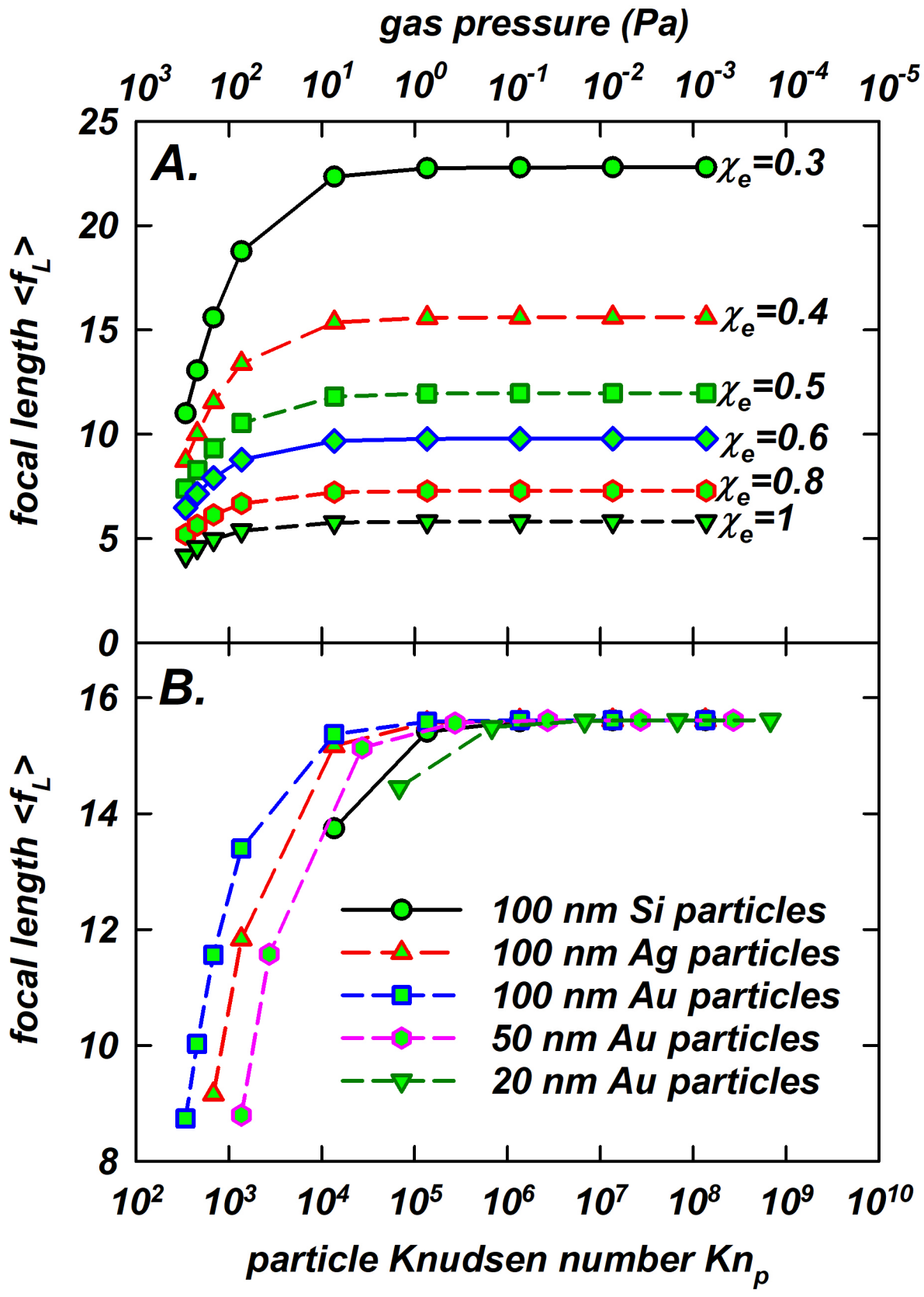
gas pressure (Pa)
10^3 10^2 10^1 10^0 10^-1 10^-2 10^-3 10^-4 10^-5
A.
χe=0.3
χe=0.4
χe=0.5
χe=0.6
χe=0.8
χe=1
focal length <fL>
25 20 15 10 5 0
B.
100 nm Si particles
100 nm Ag particles
100 nm Au particles
50 nm Au particles
20 nm Au particles
16 14 12 10 8
10^2 10^3 10^4 10^5 10^6 10^7 10^8 10^9 10^10
particle Knudsen number Knp

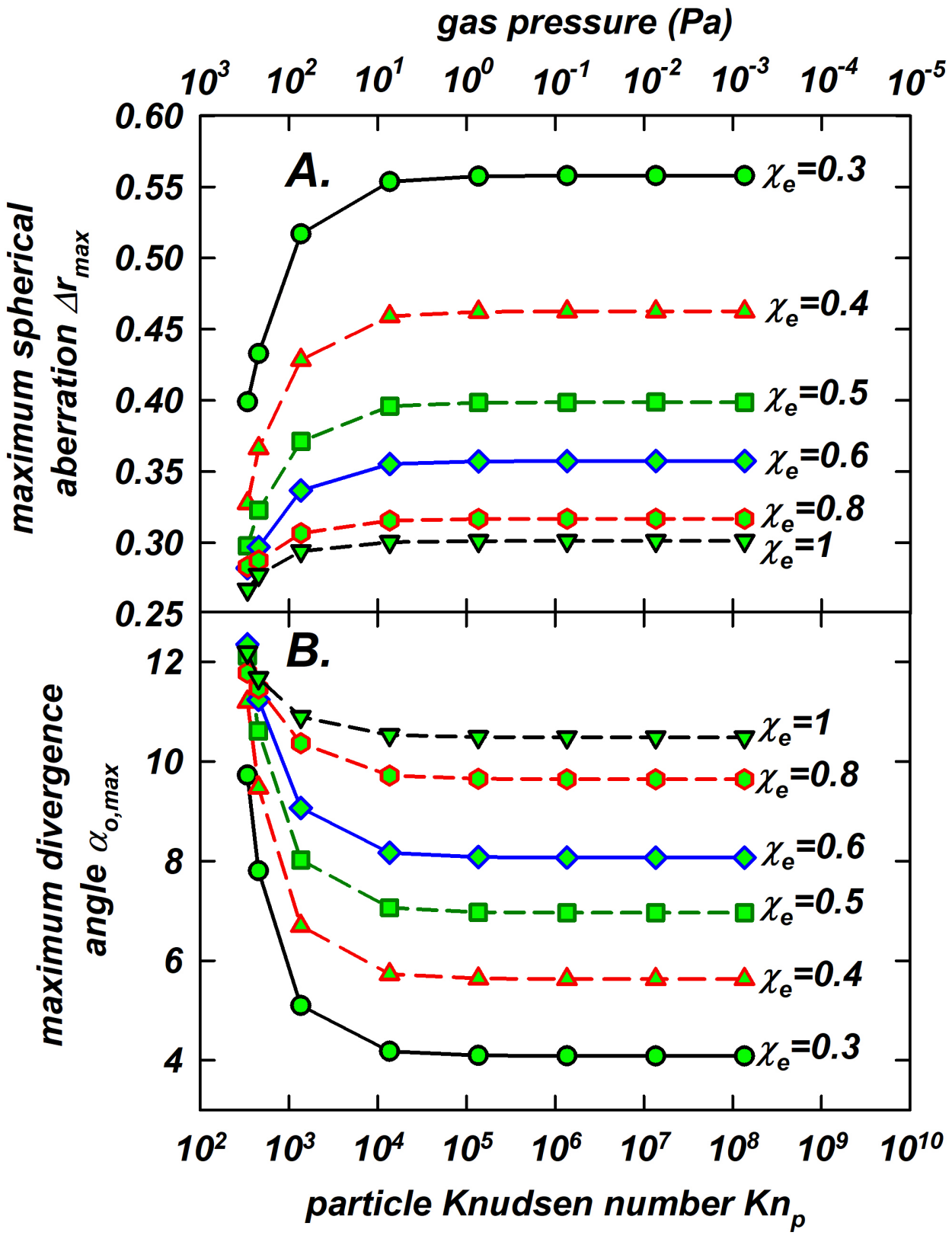
gas pressure (Pa)
10^3 10^2 10^1 10^0 10^-1 10^-2 10^-3 10^-4 10^-5
A.
maximum spherical aberration Δr_max
0.60
0.55
0.50
0.45
0.40
0.35
0.30
0.25
χe=0.3
χe=0.4
χe=0.5
χe=0.6
χe=0.8
χe=1
B.
maximum divergence angle α_o,max
12
10
8
6
4
χe=1
χe=0.8
χe=0.6
χe=0.5
χe=0.4
χe=0.3
10^2 10^3 10^4 10^5 10^6 10^7 10^8 10^9 10^10
particle Knudsen number Kn_p

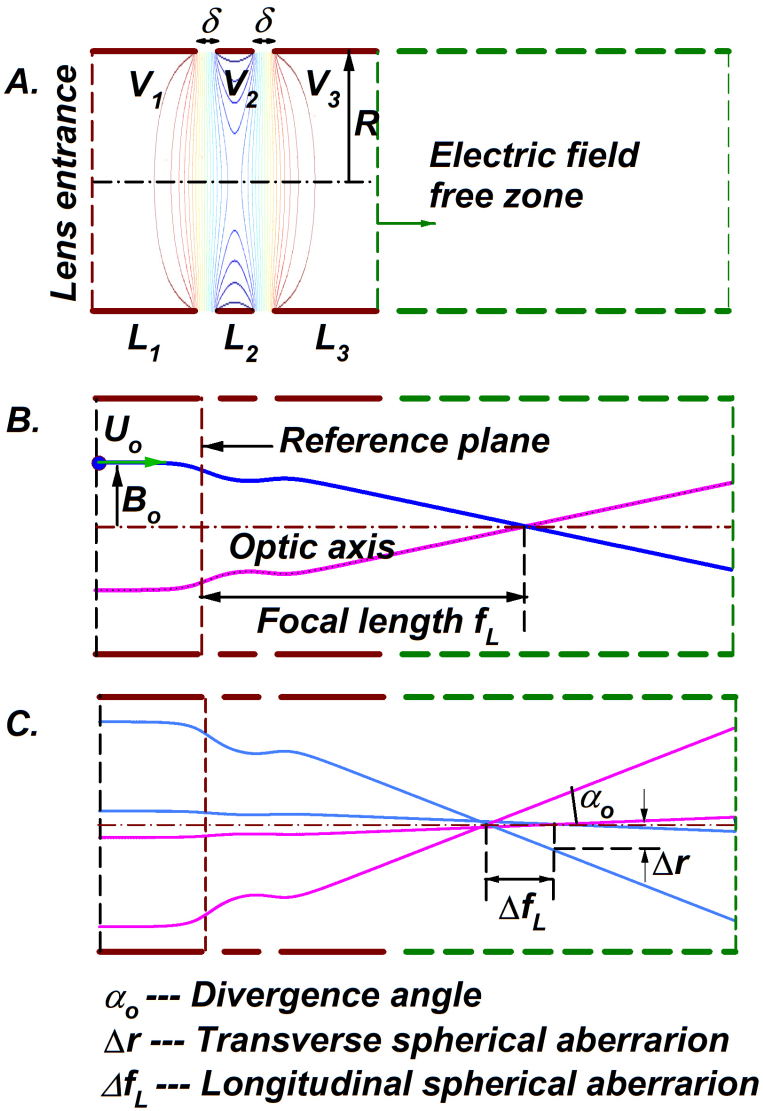

α_o --- Divergence angle

Δr --- Transverse spherical aberrarion

Δf_L --- Longitudinal spherical aberrarion

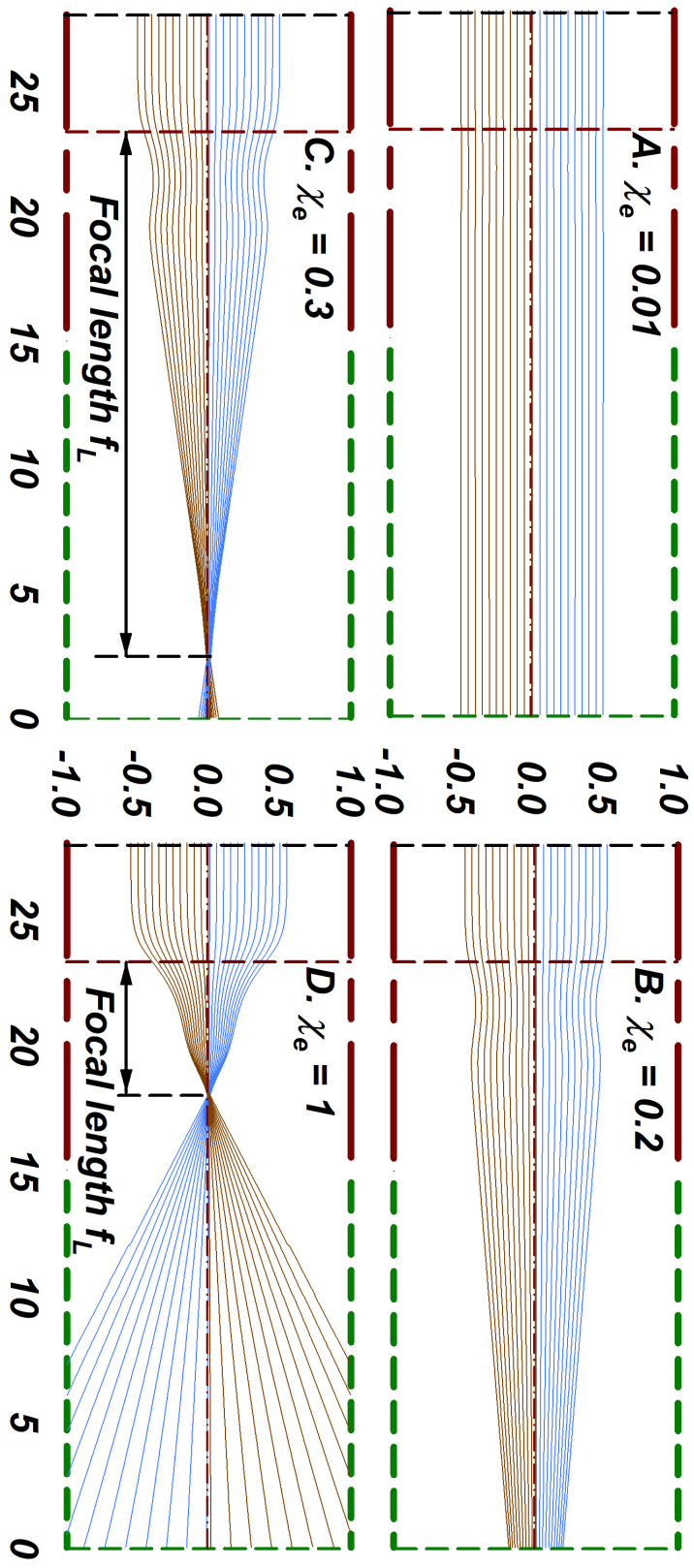
A. χ_e = 0.01
B. χ_e = 0.2
C. χ_e = 0.3
D. χ_e = 1
Focal length f_L
Focal length f_L
25
20
15
10
5
0
-1.0
-0.5
0.0
0.5
1.0

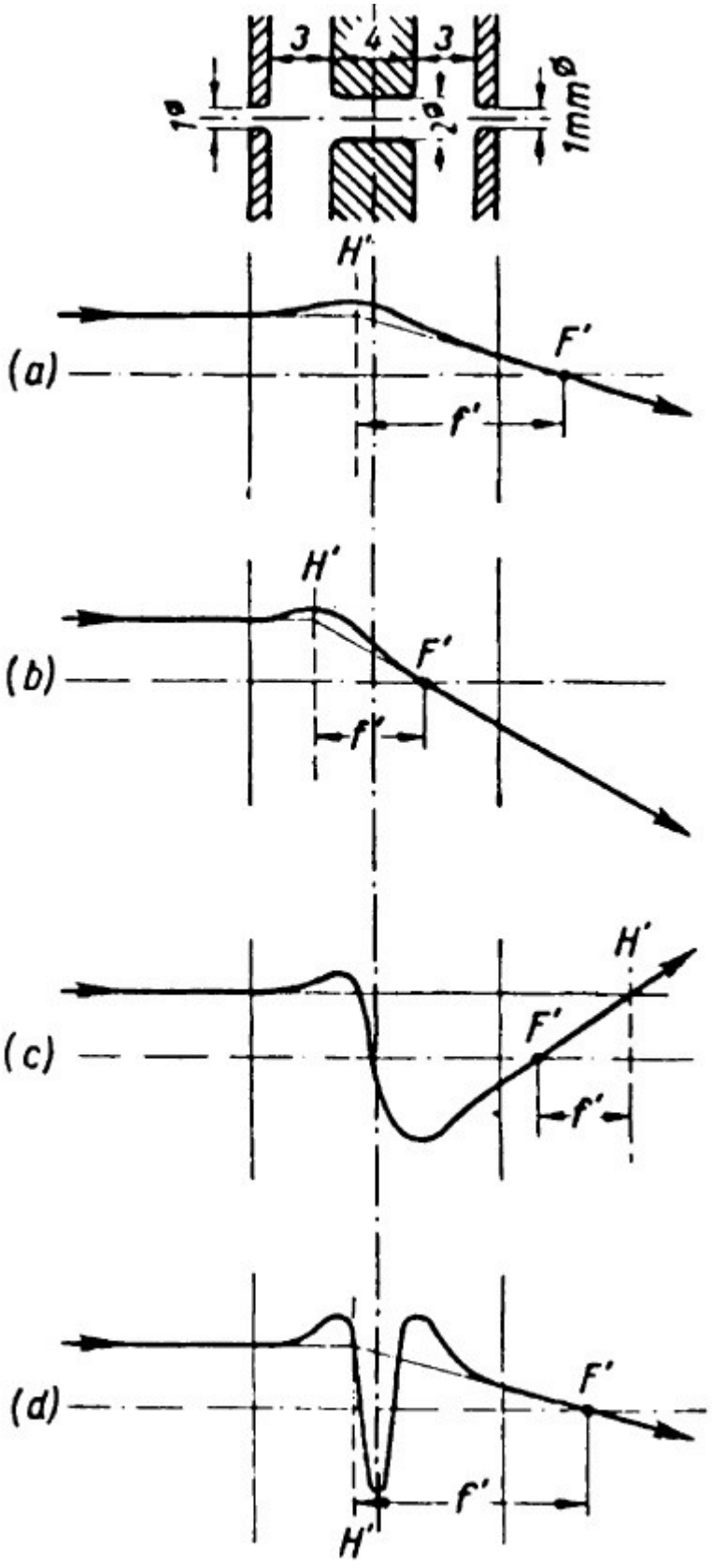
3
4
3
1
2
Ø
1mm
H'
F'
f'
(a)
(b)
(c)
(d)

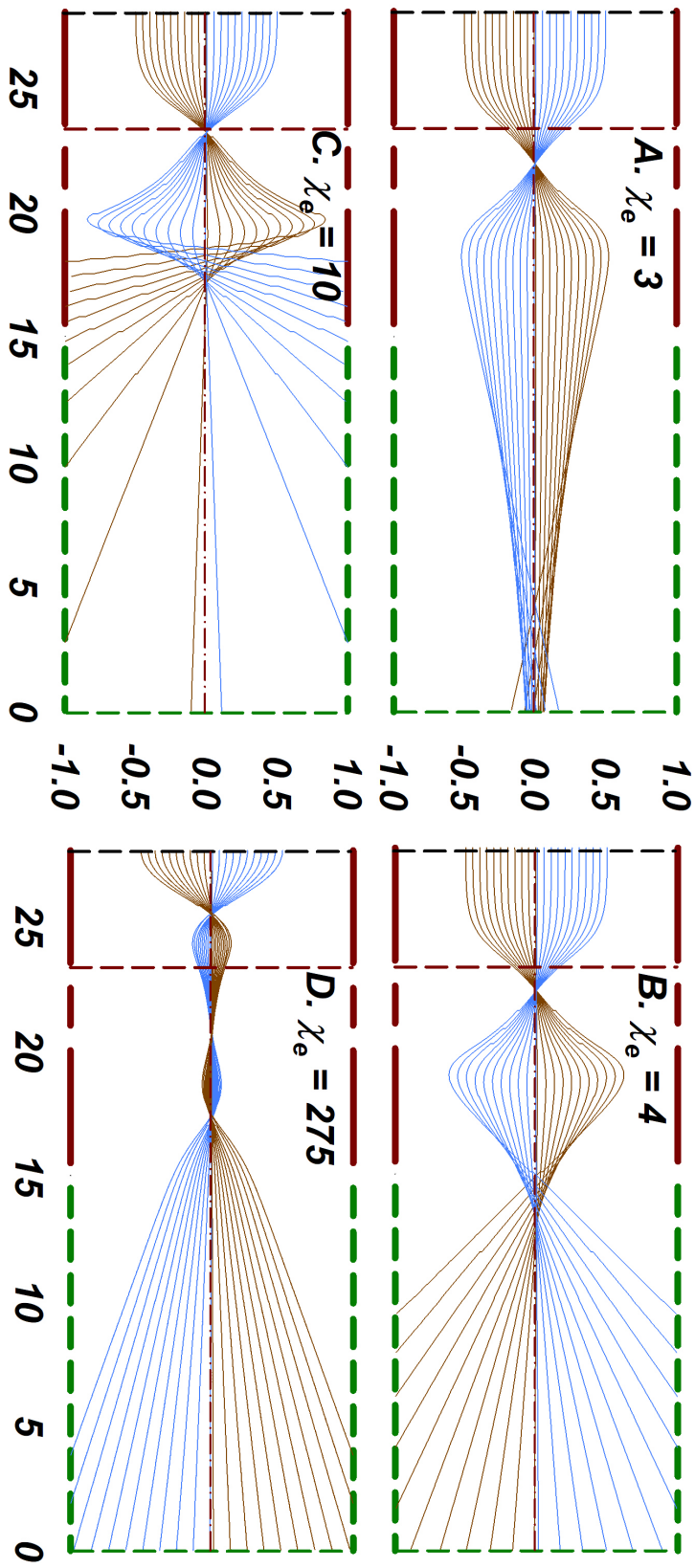
A. χ_e = 3
B. χ_e = 4
C. χ_e = 10
D. χ_e = 275
-1.0
-0.5
0.0
0.5
1.0
0
5
10
15
20
25

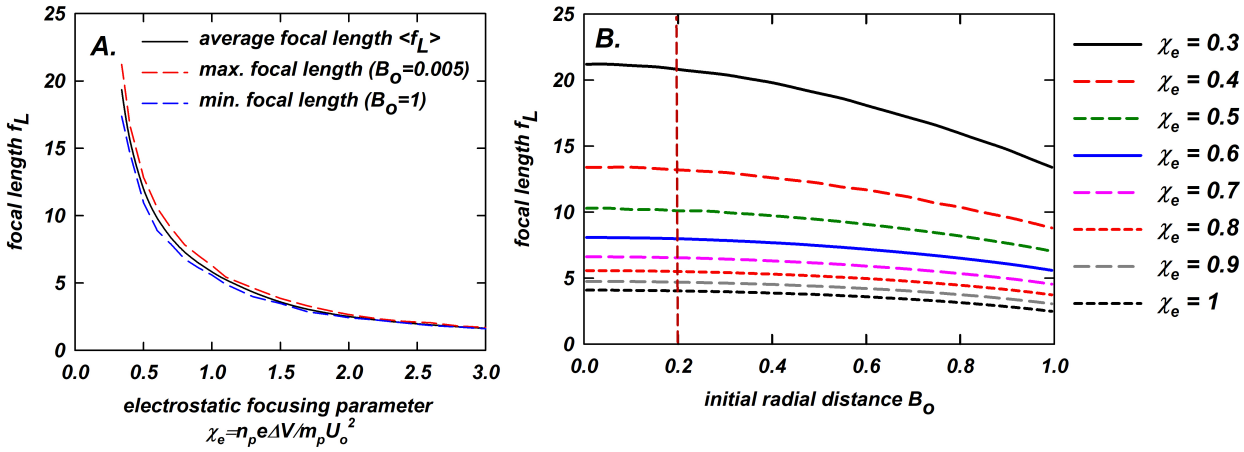

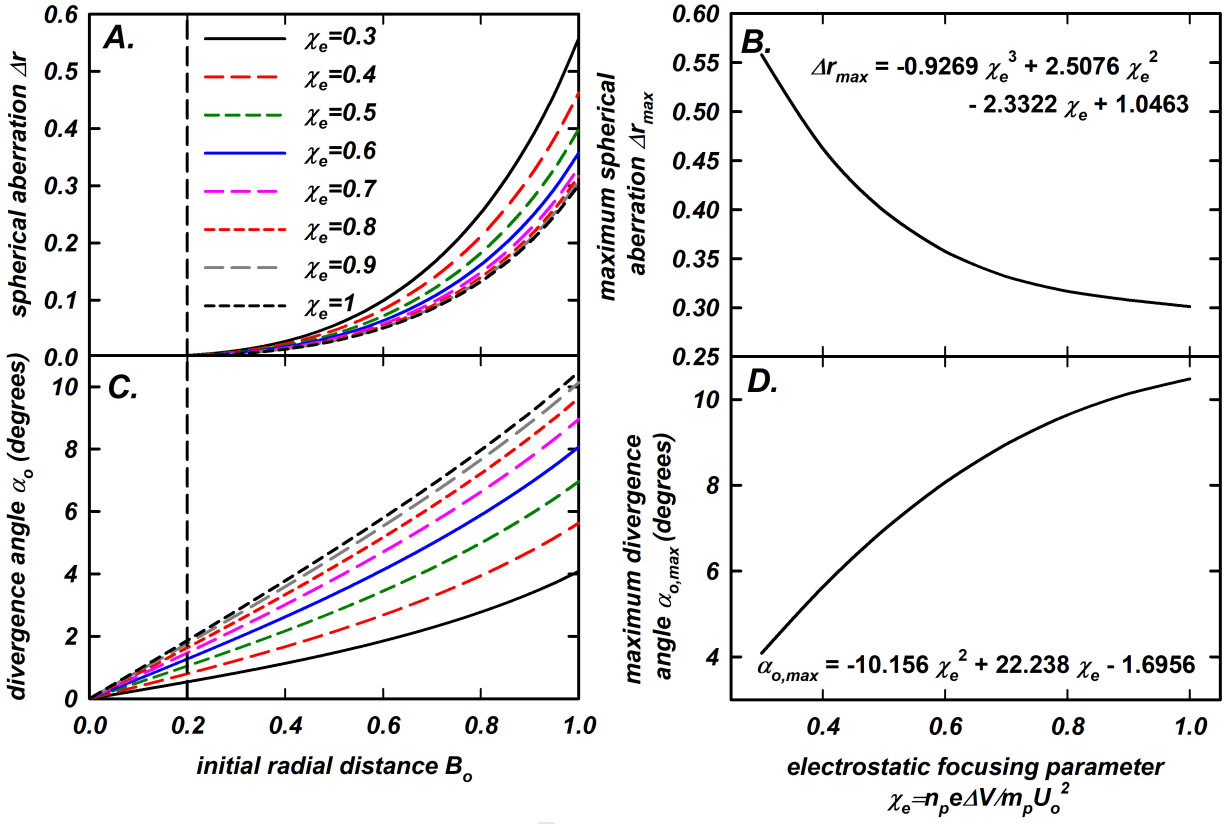
A.
B.
C.
D.
spherical aberration Δr
maximum spherical aberration Δr_max
divergence angle α_o (degrees)
maximum divergence angle α_o,max (degrees)
χ_e=0.3
χ_e=0.4
χ_e=0.5
χ_e=0.6
χ_e=0.7
χ_e=0.8
χ_e=0.9
χ_e=1
Δr_max = -0.9269 χ_e^3 + 2.5076 χ_e^2 - 2.3322 χ_e + 1.0463
α_o,max = -10.156 χ_e^2 + 22.238 χ_e - 1.6956
initial radial distance B_o
electrostatic focusing parameter
χ_e=n_p eΔV/m_p U_o^2

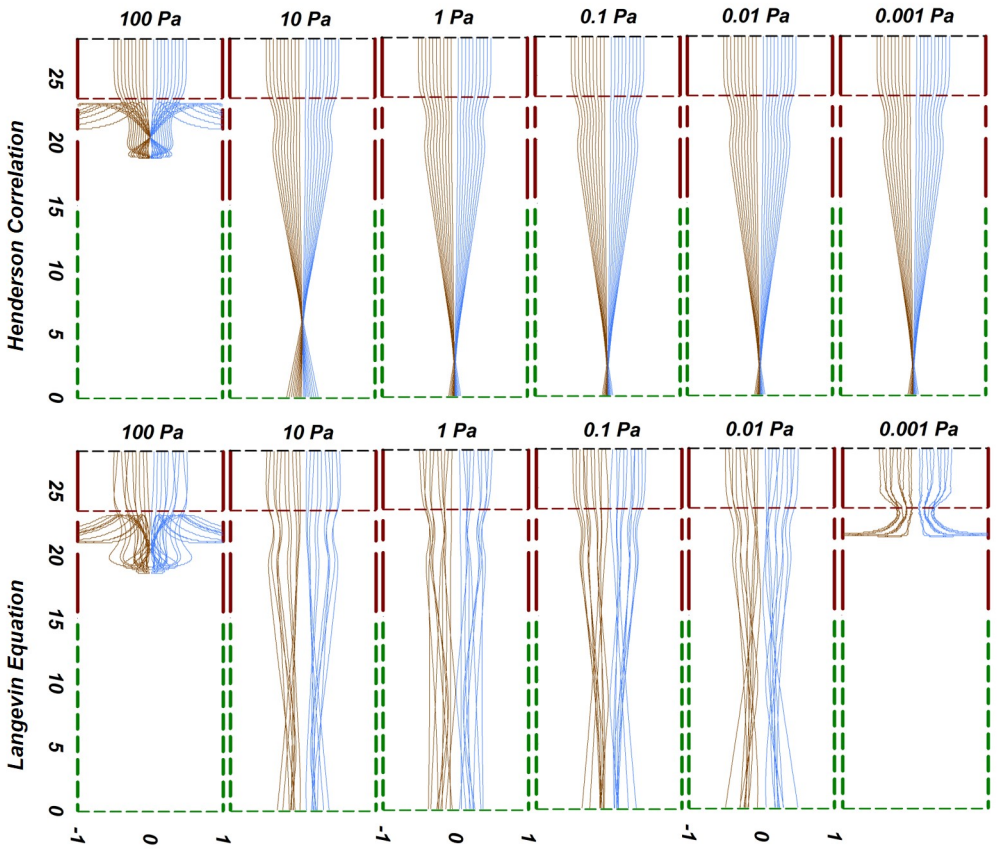
100 Pa
10 Pa
1 Pa
0.1 Pa
0.01 Pa
0.001 Pa
Henderson Correlation
Langevin Equation
0
5
10
15
20
25
-1
0
1

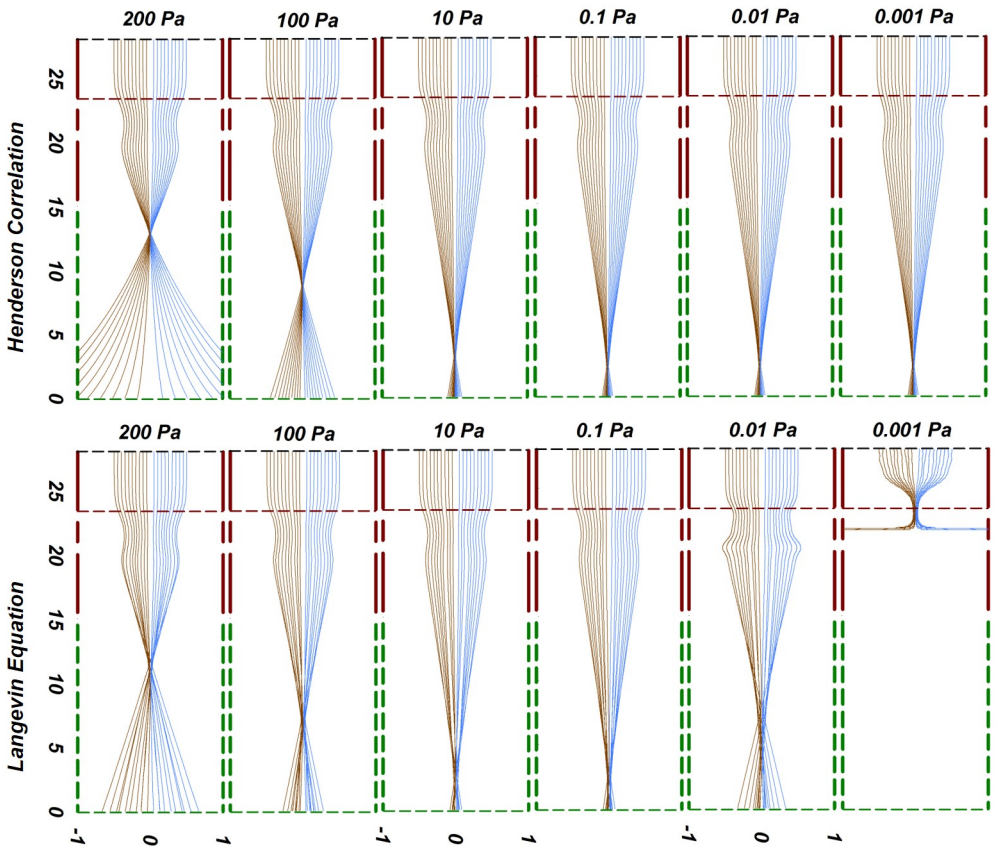
200 Pa
100 Pa
10 Pa
0.1 Pa
0.01 Pa
0.001 Pa
Henderson Correlation
Langevin Equation
0
5
10
15
20
25
-1
0
1

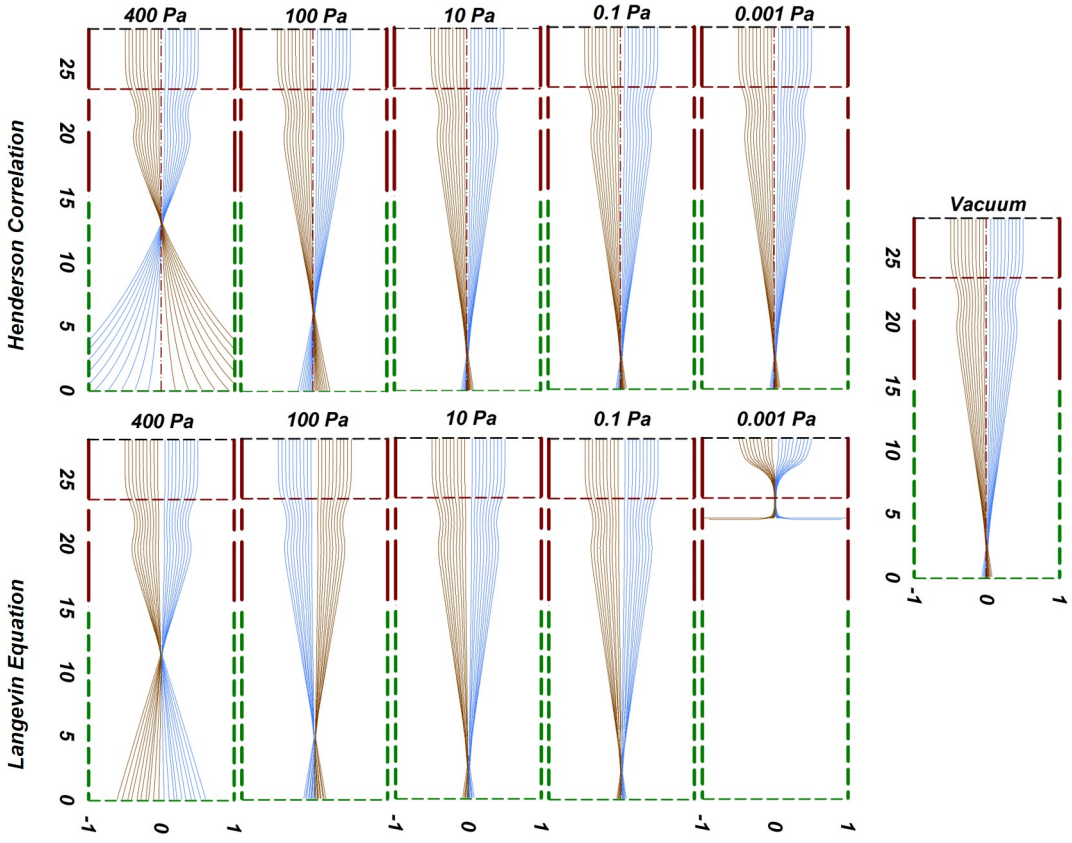
400 Pa
100 Pa
10 Pa
0.1 Pa
0.001 Pa
Henderson Correlation
Langevin Equation
Vacuum
0
5
10
15
20
25
-1
0
1

Highlights

- Trajectory simulations are used to study the focusing of aerosol nanoparticles in a 3-electrode einzel lens.
- The focusing in vacuum is greatly influenced by a ratio of electrostatic potential energy to kinetic energy χ_e.
- The focal length is seen to vary inversely with χ_e.
- Focusing performance deteriorates with increasing gas pressure.
- A maximum pressure below which the lens needs to be operated to efficiently focus particles and a minimum pressure below which the lens behaves similar to being operated in vacuum is identified.
- Considerations for successfully selecting operating parameters (χ_e and gas pressure) are discussed.

Computational study of electrostatic focusing of aerosol nanoparticles using an einzel lens

Rayhan Ahmed[1] and Ranganathan Gopalakrishnan*[1]
[1]Department of Mechanical Engineering, The University of Memphis, Memphis, TN, USA

Supplemental Information

*Corresponding author: rgplkrsh@memphis.edu, Tel: 1-901-678-2580, Fax: 1-901-678-4180

Information available: Details of trajectory calculations using the Langevin equation of motion

We model the combined electrostatic and hydrodynamic interactions of particles using the Langevin equation of motion (Langevin 1903, Chandrasekhar 1943):

$$\frac{d\vec{v}}{dt} = -St\vec{v} + \chi_e\vec{E} + \frac{\delta}{m_p U_o^2}\vec{X}(t) \ldots (S1)$$

Here, eq. S1 introduces the drag on the particles through a linear damping term $-St\vec{v}$. In addition to the non-dimensional electrostatic parameter χ_e defined in the main text, here the relative importance of particle inertia to hydrodynamic drag on particle motion is quantified through the Stokes number, $St \equiv \frac{m_p U_o}{f_p \delta}$. f_p is the friction factor that relates the hydrodynamic drag force on the particle to velocity ($drag = -f_p \cdot velocity$) in the limit of creeping flow based on the particle Reynolds number $Re_p = \frac{\rho_g U_o d_p}{\mu_g}$ $\left(Re_p \to 0\right)$. The gas parameters such as viscosity μ_g and temperature T_g describe the momentum and energy exchange between the particles and the gas medium. f_p can be readily obtained using the Stokes law for spherical particles along with the Cunningham slip correction factor C_c as $f_p = \frac{3\pi\mu_g d_p}{C_c}$. C_c has been reported by empirical correlations to measured drag on particles as a function of particle size and gas pressure in the momentum transfer transition regime (Ku and de la Mora 2009). Also, $\chi_t = \frac{k_b T_g}{m_p U_o^2}$ compares the thermal energy of the particles to their reference kinetic energy (k_b is the Boltzmann constant). The thermal fluctuations in the particle velocity and position due to impacts with gas molecules are captured by adding normally distributed random vectors $\vec{A}_v$ and $\vec{A}_x$ at each timestep. $\vec{A}_v$ and $\vec{A}_x$ have a mean of zero and variances given by equations 3c and 3d, respectively. The timestep Δt is chosen by comparing the diffusion displacement and the

electrostatic displacement of the particle as: $\Delta t = \frac{0.001}{St} \cdot \min\left(\frac{1}{\chi_e |\vec{E}(\vec{x}(t))|}, \frac{1}{\chi_t}\right)$. the factor 0.001 was chosen based on numerical experimentation to balance accuracy and computational effort to ensure that the obtained results are independent of the timestep used in the limit of $\Delta t \to 0$. By normalizing the solution to the same derived by Ermak and Buckholz (1980), we obtain the following expressions to track the velocity and position of the particles in time:

$$\vec{v}(t+\Delta t) = \vec{v}(t)\exp\left(-\frac{\Delta t}{St}\right) + \chi_e\, St\, \vec{E}\left(\vec{x}(t)\right)\left(1-\exp\left(-\frac{\Delta t}{St}\right)\right) + \vec{A}_v \ldots (S2a)$$

$$\vec{x}(t+\Delta t) = \vec{x}(t) + St\left(\vec{v}(t+\Delta t) + \vec{v}(t) - 2\chi_e St\, \vec{E}\left(\vec{x}(t)\right)\right)\left(\frac{1-\exp\left(-\frac{\Delta t}{St}\right)}{1+\exp\left(-\frac{\Delta t}{St}\right)}\right) + \chi_e St\, \vec{E}\left(\vec{x}(t)\right)\Delta t + \vec{A}_x \ldots (S2b)$$

$$\langle A_v^2 \rangle = 3\chi_t\left(1-\exp\left(-2\frac{\Delta t}{St}\right)\right) \ldots (S2c)$$

$$\langle A_x^2 \rangle = 6\chi_t St^2\left(\frac{\Delta t}{St} - 2\left(\frac{1-\exp\left(-\frac{\Delta t}{St}\right)}{1+\exp\left(-\frac{\Delta t}{St}\right)}\right)\right) \ldots (S2d)$$

Equations S2a – S2d are used in this article to elucidate particle trajectories when both hydrodynamic drag and particle Brownian motion are significant and effect focusing performance in the lens geometry described in Figure 1-A of the main text.

Chandrasekhar, S. (1943). "Stochastic Problems in Physics and Astronomy." Reviews of Modern Physics **15**: 1-89..

Ermak, D. L. and H. Buckholz (1980). "Numerical integration of the Langevin equation: Monte Carlo simulation." Journal of Computational Physics **35**(2): 169-182..

Ku, B. K. and J. F. de la Mora (2009). "Relation between Electrical Mobility, Mass, and Size for Nanodrops 1-6.5 nm in Diameter in Air." Aerosol Science and Technology **43**(3): 241-249..

Langevin, P. (1903). Ann. Chim. Phys. **28**: 289..